

Discerning Torquoselectivity of Non-Competitive and Competitive Ring-Opening Reactions Using QTAIM and Stress Tensor

Roya Momen¹, Alireza Azizi², Alejandro Morales-Bayuelo³, and Xiaobo Ji¹

¹Central South University

²Hunan Normal University

³Universidad del Sinú

June 17, 2021

Abstract

Within this study, four thermal ring-opening reactions, Reactions (1-4), were selected in order to investigate the phenomenon of torquoselectivity as well as predicting non-competitive or competitive reactions in QTAIM and stress tensor frameworks rather than using conventional methods. The theoretical analysis for these reactions exhibits differently for non-competitive and competitive reactions as well as for the conrotatory preferences either TSOC or TSIC directions by presenting degeneracy or non-degeneracy in their results. The concordant results of stress tensor and QTAIM scalar and vectors with experimental results provide a better understanding of all reactions mechanism. Examination the $\xi(\mathbf{r}_b)$, ϵ , $H(\mathbf{r}_b)$, P_σ , $\lambda_{3\sigma}$, BPL, and H indicate that Reaction 1 is a competitive and Reactions (2-4) are non-competitive reactions with TSOC, TSOC, and TSIC preference directions respectively.

Discerning Torquoselectivity of Non-Competitive and Competitive Ring-Opening Reactions Using QTAIM and Stress Tensor

Roya Momen ^{*1}, Alireza Azizi ^{2,3}, Alejandro Morales-Bayuelo ⁴, Xiaobo Ji ^{*1}

¹ State Key Laboratory of Powder Metallurgy, College of Chemistry and Chemical Engineering, Central South University Changsha, 410083, China.

² College of Material Science and Engineering, Central South University, Changsha, Hunan 410083, China

³ College of Chemistry and Chemical Engineering, Hunan Normal University, Changsha, Hunan 410081, China

⁴ Grupo GENOMA, Escuela de Medicina, Universidad del Sinú-EBZ, Cartagena, Colombia

E-mail: roya-momen@csu.edu.cn

E-mail: xji@csu.edu.cn

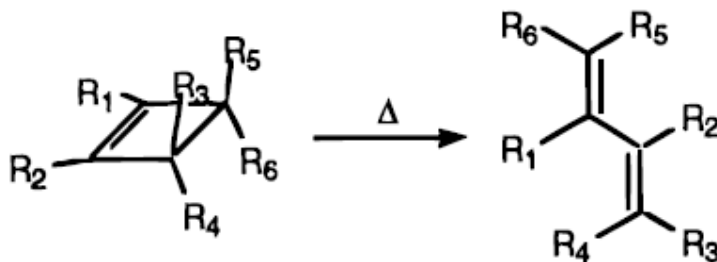
Within this study, four thermal ring-opening reactions, **Reactions (1-4)**, were selected in order to investigate the phenomenon of torquoselectivity as well as predicting non-competitive or competitive reactions in QTAIM and stress tensor frameworks rather than using conventional methods. The theoretical analysis for these reactions exhibits differently for non-competitive and competitive reactions as well as for the conrotatory preferences either TSOC or TSIC directions by presenting degeneracy or non-degeneracy in their results. The concordant results of stress tensor and QTAIM scalar and vectors with experimental results provide a better understanding of all reactions mechanism. Examination the $\xi(\mathbf{r}_b)$, ϵ , $H(\mathbf{r}_b)$, P_σ , $\lambda_{3\sigma}$, BPL, and H

indicate that **Reaction 1** is a competitive and **Reactions (2-4)** are non-competitive reactions with TSOC, TSOC, and TSIC preference directions respectively.

Keywords: Quantum Theory of Atoms in Molecules, Transition State Inward/Outward Conrotatory, Ring-Opening Reaction, Bond Critical Points, Intrinsic Reaction Coordinate.

1. Introduction

It has been several development studies about torquoselectivity during recent years. This property can be defined as the preference by the outward or inward of the substitutes in the electrocyclic ring-opening reactions¹⁻⁶. Traditionally, this property has been aboard into the Woodward-Hoffmann rules using the orbital symmetry^{7,8}. The studies using the Woodward-Hoffmann rules in electrocyclic reactions establish a relationship between electrocyclic ring-opening reactions with an electronic reorganization thought pericyclic process. However, in several reactions it pericyclic reorganization cannot explain the experimental data in electrocyclic reactions or reaction yields. Therefore, new points of view beyond orbital symmetry is necessary⁹⁻¹⁶.



During recent years our research group has studied the nature of chemical bonds using the background studied by Silvi and collaborators using the bond progression theory as an extension of Bader's work and the scalar field related to the electron localization function (ELF)¹⁷⁻²³. These studies have proposed the electronic reorganization as a pseudo radical process instead pericyclic process suggested by Woodward-Hoffmann rules²⁴⁻²⁶. Additionally, we use the analysis of natural bond orbitals (NBO), the quantum theory of atoms in molecules (QTAM), and the electronic structure principles such as minimum polarizability, minimum electrophilicity and, maximum hardness presenting new insights into the process of electronic reorganization agree with experimental data²⁷⁻³⁰.

Scheme 1. Ring-opening reaction of Cyclobutenes studied

Table 1. Thermal ring-opening reaction of cyclobutenes, the reaction set analyzed in this study.

Relative Energy (Kcal/mol) ^T*S*ReactionReactant(substituents)TSIC TSOC (TSIC-TSOC) Stereochemistry Ref.

R1 1-chlorocyclobut-1-ene 41.425 41.425 0.000 —³¹

R2 3-chloro-4-methylcyclobut-1-ene 49.411 42.642 +6.769 *E,Z*³²

R3 3-chloro-4-methoxycyclobut-1-ene 53.973 42.763 11.210 *E,Z*³²

R4 3-methoxy-4-methylcyclobut-1-ene 44.794 51.323 -6.529 *E,E*³²

Table 1 shows the reaction set analyzed in this study (see Figure 1). There is molecular variety in the reaction set analyzed from reactions without stereochemistry and competitive reactions with *E, Z* stereochemistry. The main aim is to build a systematic study to understand the nature of the chemical bond, electronic reorganization, and stereochemistry prediction according to the experimental data.

2. Theory and Methods

Quantum Theory of Atoms in Molecules (QTAIM)³³ known as a comprehensive topology interpretation tool of quantum mechanics, provides a method to explore the distribution of electrons $\rho(\mathbf{r})$, returning a comprehensive quantitative analysis of the atom's bonding environments in a molecule. In the scalar field $\rho(\mathbf{r})$, we can define a piecewise continuous gradient path by evaluating $[\nabla]\rho(\mathbf{r})$ at some points and then tracking this vector for a very short distance and re-evaluating $[\nabla]\rho(\mathbf{r})$. An atom is an area of real space bounded by surfaces in which there is zero flux in the total electronic charge density distribution's gradient vector field. The interaction surface is defined by the set of trajectories ending at the point where $\rho(\mathbf{r}) = 0$, which implies that the zero-flux boundary conditions are satisfied by an interatomic surface: $[\nabla]\rho(\mathbf{r}) \cdot \mathbf{n}(\mathbf{r}) = 0$. Where $\mathbf{n}(\mathbf{r})$ is the unit vector common to the surface at \mathbf{r} since the surface is not crossed by any of the trajectories of $\rho(\mathbf{r})$. The charge density $\rho(\mathbf{r})$ is a physical quantity with a particular value at each point in space, and the forces exerted on it by the nuclei dominate a topological structure. We may distinguish between various forms by examining the properties of the Hessian matrix of $\rho(\mathbf{r})$ at each critical point. The ordered eigenvalue set $\lambda_1 < \lambda_2 < \lambda_3$ is obtained by diagonalizing the Hessian matrix of $\rho(\mathbf{r})$, and the algebraic sum of these eigenvalues is the Laplacian of the electron density. In addition, these three eigenvalues are corresponding with a set of eigenvectors e_1, e_2, e_3 . Analyzing the eigenvalues of the Hessian matrix of $\rho(\mathbf{r})$ are used to determine whether the forces exerted by and on the (\mathbf{r}) favor tensile modes, such as expansion or compression for the volume element relevant to the positive or negative eigenvalue. An atomic interaction line (AIL)³⁴ becomes a bond-path, but not permanently a chemical bond³⁵, when the forces on the nuclei become vanishingly small.

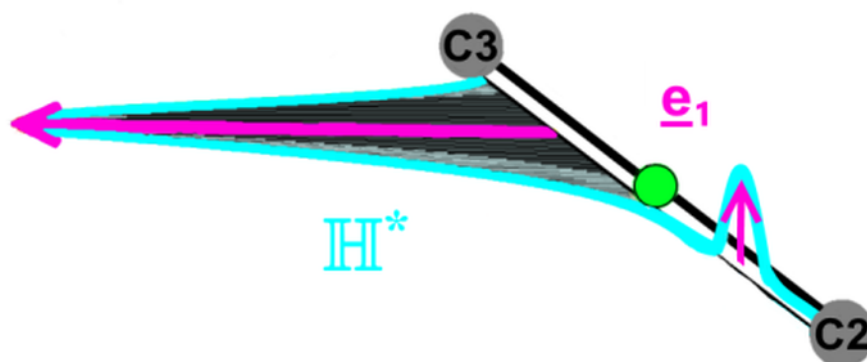
Bond ellipticity is defined by $\epsilon = |\lambda_1|/|\lambda_2| - 1$ is providing the relative accumulation of the two perpendicular axes of the Hessian matrix, negative λ_1 and λ_2 eigenvalues, to the bond-path at a *BCP*³³. Metallicity, $\xi(\mathbf{r}_b) = \rho(\mathbf{r}_b)/[\nabla]^2\rho(\mathbf{r}_b)$ is one of the correlated quantity to the ellipticity ϵ for closed-shell interactions $[\nabla]^2\rho(\mathbf{r}_b) > 0$. Where $[\nabla]^2\rho(\mathbf{r}_b)$ and $\rho(\mathbf{r}_b)$ are Laplacian and the values of total electronic charge density at the *BCP* respectively. The $\xi(\mathbf{r}_b)$ is an important indicator for the ring-opening reactions bond path^{36,37} while the relative values of $\rho(\mathbf{r}_b)$ and $[\nabla]^2\rho(\mathbf{r}_b)$ seem to alter at a *BCP* as the bond path stretched as long as eventually ruptured. Therefore $\xi(\mathbf{r}_b)$ will relate to the reaction electronic flux (REF, $J(\xi)$), which corresponding to a chemical process along with the IRC(ξ) and is defined to be $J(\xi) = -d\mu/d\xi$ ³⁸ Where μ is the chemical potential. The use of the Greek letter 'ξ' for the metallicity $\xi(\mathbf{r}_b)$ and REF $J(\xi)$ definitions is purely coincidental. Although previously metallicity has been used to consider suspected metallicity ranges of metalloids, metals, and non-metals^{36,37}, other researchers represent that $\xi(\mathbf{r}_b)$ is conversely associated with "nearsightedness" of the first-order density matrix and is appropriate for closed-shell systems³⁹.

The total local energy density, $H(\mathbf{r}_b) = G(\mathbf{r}_b) + V(\mathbf{r}_b)$, could determine The presence of a degree of covalent character^{40,41} where $G(\mathbf{r}_b)$ and $V(\mathbf{r}_b)$ are the local kinetic and potential energy densities respectively at a *BCP*. Precisely a degree of covalent character and a degree of lack of covalent character for a closed-shell interaction, $[\nabla]^2\rho(\mathbf{r}_b) \leq 0$, where a value of $H(\mathbf{r}_b) < 0$ and $H(\mathbf{r}_b) > 0$ respectively. Stress tensor stiffness $S_\sigma = |\lambda_{1\sigma}|/|\lambda_{3\sigma}|$ is the other proper descriptor of the resistance of the bond path to the applied distortion. It follows the similar trend with ellipticity ϵ , where double and single bonds indicate by $\epsilon > 0.25$ and lower values respectively, as is expected the single bond is less resistant to torsion than a double bond. P_σ display the stress tensor polarizability, $P_\sigma = |\lambda_{3\sigma}|/|\lambda_{1\sigma}|$, which could define the reciprocal of the stress tensor stiffness S_σ ⁴²⁻⁴⁴.

The length of the path followed out by the e_3 eigenvector of the Hessian of the total charge density $\rho(\mathbf{r})$ that is passing through the *BCP* along which $\rho(\mathbf{r})$ is locally maximal regard

to any neighboring paths, is known as the bond-path length (BPL). Moreover, the bond-path curvature, $(\text{BPL} - \text{GBL})/\text{GBL}$, is defined as the dimensionless ratio that separates two bonded nuclei. Where BPL and GBL have associated bond-path length and the inter-nuclear separation, respectively. Notice that particularly for strained or weak bonds and strange bonding environments usually BPL exceeds the GBL⁴⁵. According to the hypothesis that a bond-path may possess 1-D, 2-D, or a 3-D morphology^{46,47} with 2-D or a 3-D bond-paths corresponding to a *BCP* with ellipticity $\epsilon > 0$, is because of differing degrees of charge density accumulation of the λ_2 and λ_1 eigenvalues respectively.

By Starting with utilizing the ellipticity as the scaling factor, we choose the length traced out in 3-D by the path swept by the tips of the scaled e_2 eigenvectors of the λ_2 eigenvalue. With n scaled eigenvectors e_1 tip path points $p_i = r_i + \epsilon_i e_{1,i}$ on the path p where $\epsilon_i =$ ellipticity at the i^{th} bond-path point r_i on the bond-path r . In accordance with the e_2 tip path points, we have $\chi_1 = \rho_i + \epsilon_i e_{2,i}$ on the path q where $\epsilon_i =$ ellipticity at the i^{th} bond-path point r_i on the bond-path r .



It is worth noting that the bond path, which is correlated with the λ_3 eigenvalues of the e_3 eigenvector, does not take into consideration contrasts within λ_2 and λ_1 eigenvalues of the e_2 and e_1 eigenvectors. The *bond-path framework set* indicated by $B = \{p, q, r\}$ will be used, which demonstrates the new QTAIM interpretation of the chemical bond. This viably implies that in the most well-known cases, a bond is comprised of three ‘linkages’; p , q , and r associated with the e_1, e_2 , and e_3 eigenvectors, individually. Subsequently, Scheme 1 clearly illustrates that the p parameter interprets eigenvector-following paths with lengths $\mathbb{H} = \sum_{i=1}^{n-1} |q_{i+1} - q_i|$ whilst the q parameter interpret eigenvector-following paths with lengths $\mathbb{H}^* = \sum_{i=1}^{n-1} |p_{i+1} - p_i|$. The scaled e_1 or e_2 eigenvectors will sweep out alongside the extent of the bond-path, specified by the e_3 eigenvector, between the two bonded nuclei that the bond-path interfaces, resulting in *eigenvector-following paths* with lengths \mathbb{H}^* or \mathbb{H} . For shared-shell *BCP* s From the forms of p and q , we observed that within the constrain of the ellipticity ϵ [?] 0 comparing to single bonds, as a result, we obtain the $p_i = q_i = r_i$, the value of the lengths \mathbb{H} and \mathbb{H}^* reaches its lowest point; the bond-path length (r) BPL. In contrast, for double bonds which have higher values of the ellipticity ϵ , results show in values of \mathbb{H}^* and $\mathbb{H} > \text{BPL}$. Moreover, $\mathbb{H} = \mathbb{H}^*$ if identical scaling factor ϵ_i is used in their equations since \mathbb{H}^* and \mathbb{H} are defined by the distances swept out by the e_1 and e_2 tip path points respectively.

(a) (b)

Scheme 2. in sub-figure (a) the red curve line corresponds to the \mathbb{H} , constructed from the path swept out by the tips of the scaled e_2 eigenvectors, shown in mid blue, and is defined by the equation mentioned in section 2.2. In sub-figure (b) the pale blue curve line corresponds to the \mathbb{H}^* , constructed from the path swept out by the tips of the scaled e_1 eigenvectors,

shown in magenta, and is defined by the equation mentioned in section 2.2. The mid-blue and magenta arrows representing the e_2 and e_1 eigenvectors are scaled by the ellipticity ϵ respectively, where for visualization purposes the vertical scales are magnified. The green sphere shows the position of a given BCP ⁴⁸.

3. Computational details

The reactions selected were studied using the forward (f) and reverse (r) intrinsic reaction coordinate (IRC) path. In each reaction was calculated the transition states. The transition states were revised in order to present one and only one negative eigenvalue of the energy second derivative matrix and the associated characteristic negative frequency. In the computational protocol was generated several sets of atomic positions correspond to the calculated points on the IRC. The last generated structures on the end of each calculated IRC path were then further geometry optimized to local minimum energy structures. All IRC calculations were developed with mass-weighted coordinates and the reaction path step-size used in all cases was the default value of 0.1 amu^{1/2}-Bohr. Finally, on each point on each IRC path (including the end minima), single-point calculations were generated the necessary density information. All calculation data were carried out using DFT B3LYP/6-311+G(d,p) with the Gaussian 09vD.01⁴⁹ program. The stability of all calculations generated were checked using the wave functions to perturbations including spin restricted - unrestricted perturbations and were found to be stable. Finally, the QTAIM and stress analysis was performed with the AIMAll ⁵⁰ suite on the wave function obtained.

4. Results and Discussions

In this investigation, we will determine whether a reaction is non-competitive or competitive as well as distinguish the torquoselectivity along the reaction coordinate of given reactions in order to understand either TSIC or TSOC preferences. To begin with, we propose to use chemical topological properties of reactions instead of using a universally conventional method, which is based on activation energy, see Table 1 and Figures (1-4(c)). According to [?] $TS < 1.0$ kcal/mol shown in this table results that Reaction 1 is competitive while the other three reactions, Reactions (2-4), are non-competitive reactions. As mentioned earlier, we decide to use some plots such as, metallicity $\xi(r_b)$, stress tensor polarizability P_σ , ellipticity ϵ , total local energy density $H(r_b)$, and stress tensor $\lambda_{3\sigma}$ that contain chemical topological properties of reactions. From the examination of these plots, consider that the TSIC and TSOC reactions of the ring-opening C2-C3/C2-C3 BCP s of Reactions (1-4) exhibit degeneracy or non-degeneracy that could assist in predicting either non-competitive or competitive reactions, see Figures (1-4). The plots of the variation of the metallicity $\xi(r_b)$ with the IRC related to the ring-opening C2-C3/C2-C3 BCP s, found for $\xi(r_b) > 1$, indicate degeneracy for Reaction 1 and non-degeneracy for remain reactions, Reactions (2-4), see Figures (1-4(d)) respectively. This degenerate and non-degenerate behavior in the metallicity $\xi(r_b)$ suggests that in fact Reaction 1 is a competitive reaction and Reaction 2, Reaction 3, and Reaction 4 are non-competitive reactions on the chemical basis of metallicity being a key factor in understanding the electronic reorganization of the ring-opening BCP along the reaction pathways. In addition, based on the transition state theory and previous researches outcomes, we obtain that for all four reactions, the transition state and maximum metallicity $\xi(r_b)$ relevant to the ring-opening C2-C3/C2-C3 BCP s do not simultaneously occur ⁴⁸. Subsequently, the degeneracy results from other QTAIM measures such as ellipticity ϵ and the total local energy density $H(r_b)$ are in confirmation with metallicity $\xi(r_b)$ results which indicate that Reaction 1 is a competitive reaction and Reaction 2, Reaction 3, and Reaction 4 are non-competitive reactions, see Figures (1-4(e)) and Figures (1-4(f)) respectively.

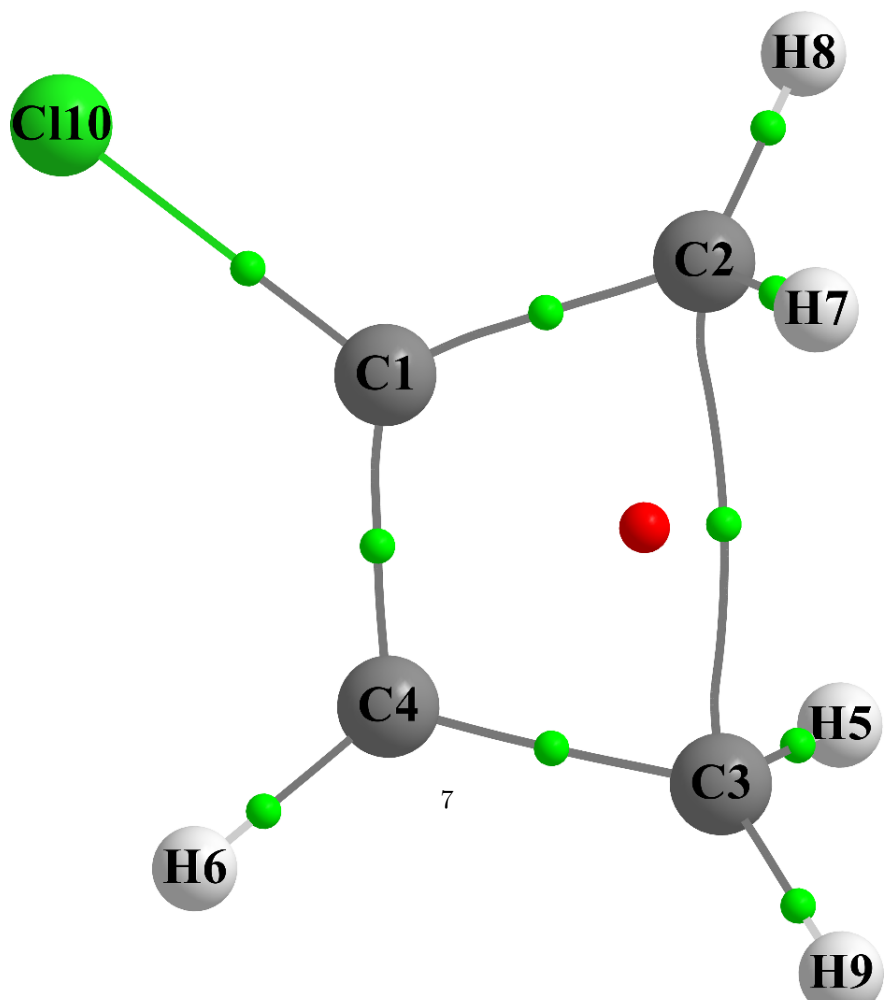
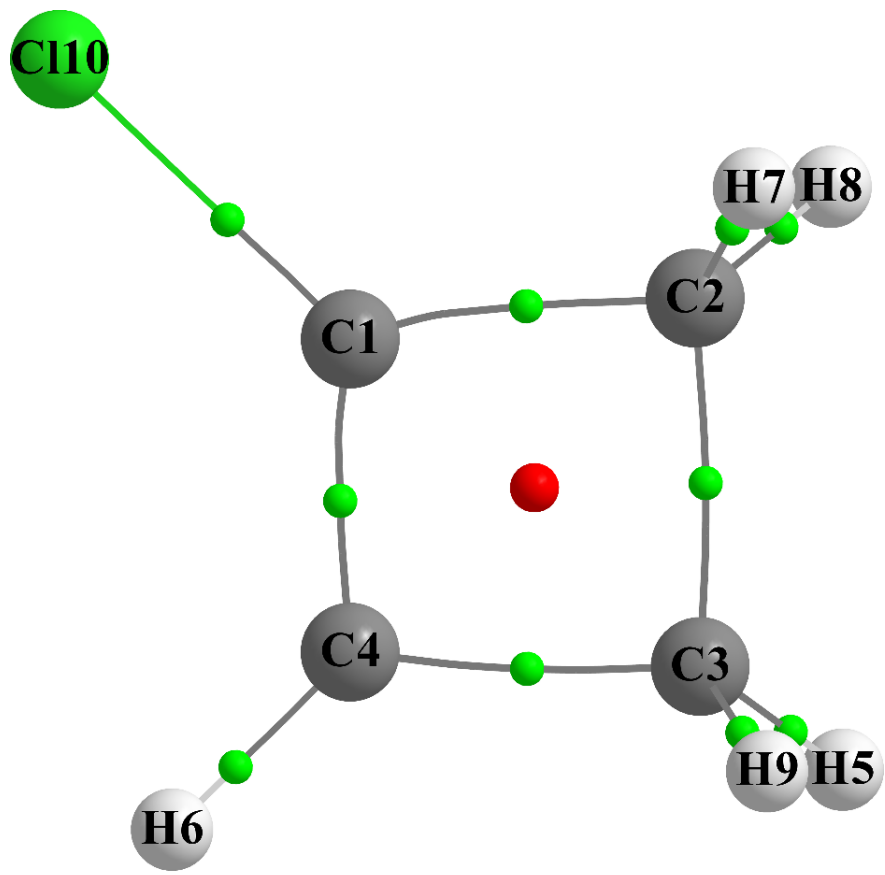
In the following, investigation the plots of variation of stress tensor polarizability P_σ with the IRC demonstrate an apparent differentiation among all four reactions. In other words, we can

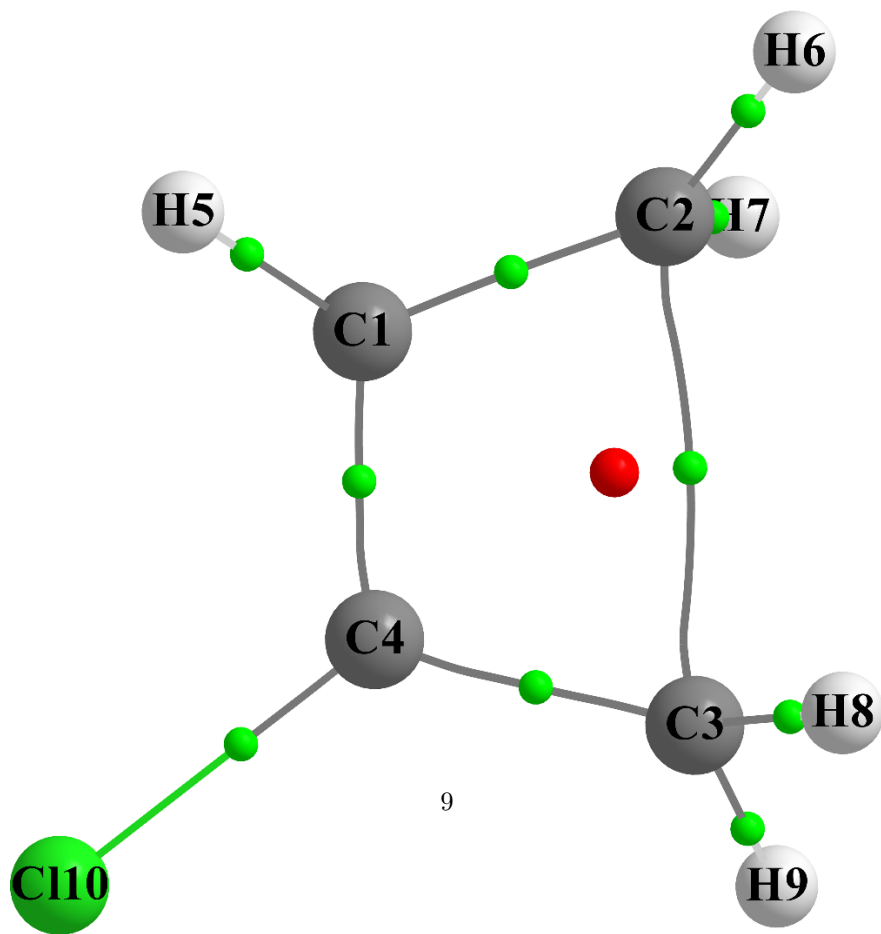
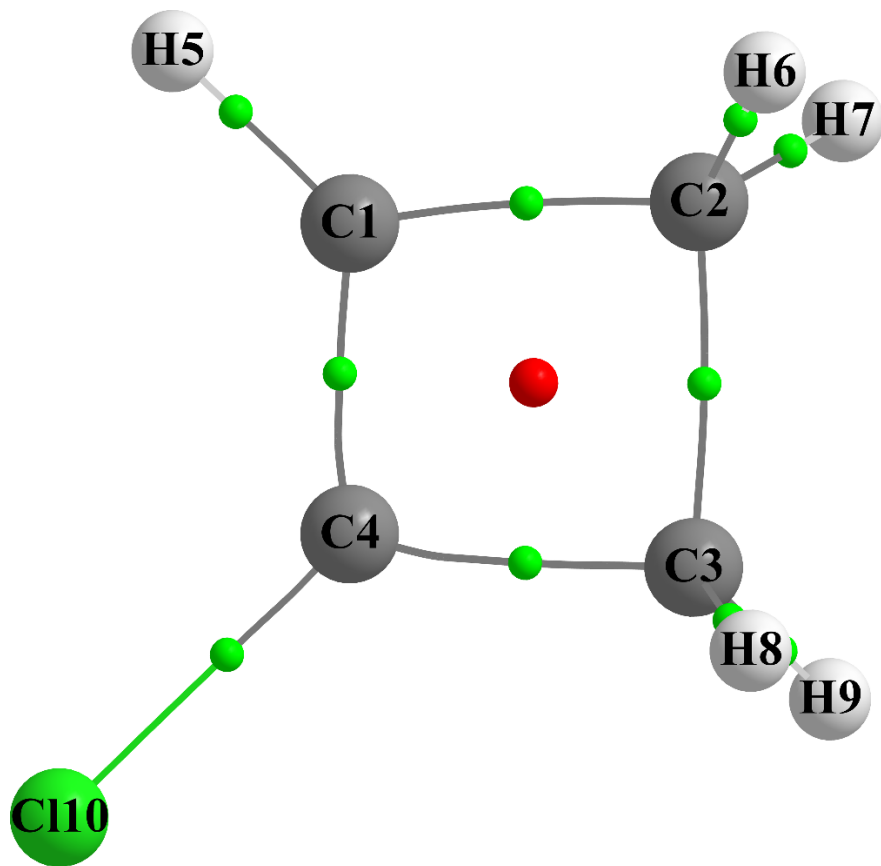
conclude from the degenerate and non-degenerate behavior of the stress tensor polarizability P_σ corresponding to the ring-opening C2-C3/C2-C3 *BCP* s that Reaction 1 is a competitive reaction and Reaction 2 , Reaction 3 , and Reaction 4 are non-competitive reactions, see Figures (1-4(g)) . Additionally, we obtain the same behavior as was happened for the metallicity $\xi(r_b)$ that the saddle point and transition state do not coincide precisely with each other. Moreover, the plots of examination of the variation of the stress tensor $\lambda_{3\sigma}$ with the IRC for all four reactions are considered which display similar evaluation with QTAIM measures mentioned above; see Figures (1-4(h)) .

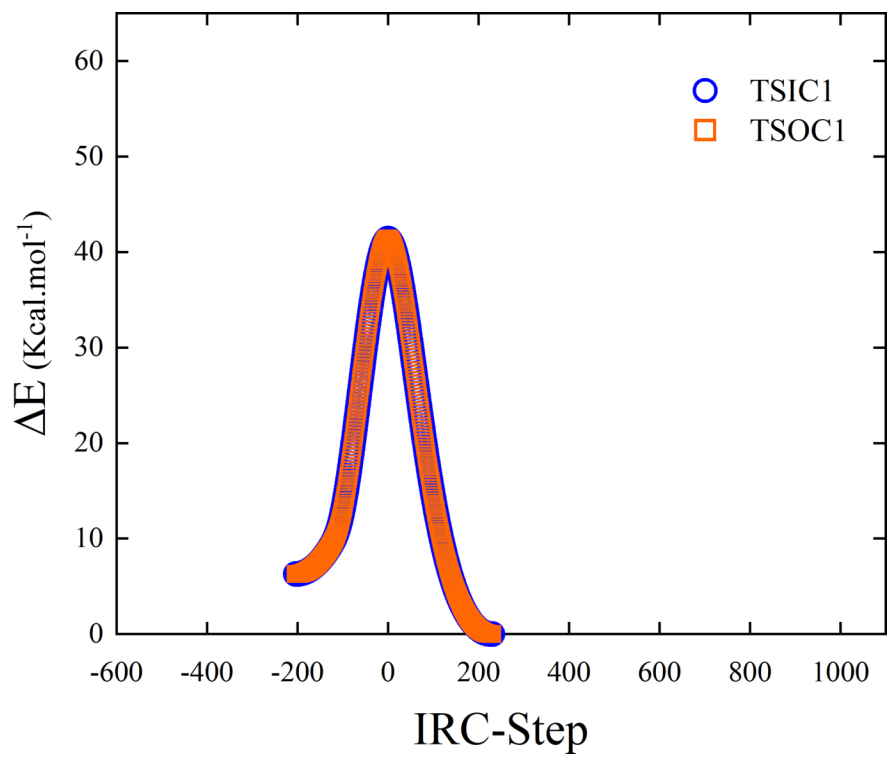
From this part of our survey, we can conclude that besides activation energy which is a conventional method, we introduce some different measures such as, $\xi(r_b)$, $\epsilon, H(r_b)$, P_σ , $\lambda_{3\sigma}$, which could be suitable indicators to predict that each reaction is non-competitive or competitive.

Inspired by the theoretical predictions, we decided to evaluate the tendency of each non-competitive reaction to determine if it is either TSIC or TSOC reactions. Hence, using the eigenvector-following path with length, which is nominated as helicity length H relevant to the shared-shell ring-opening *BCP* of each of the Reactions (1-4) pathways was determined, see Figures (1-4(j)) respectively.

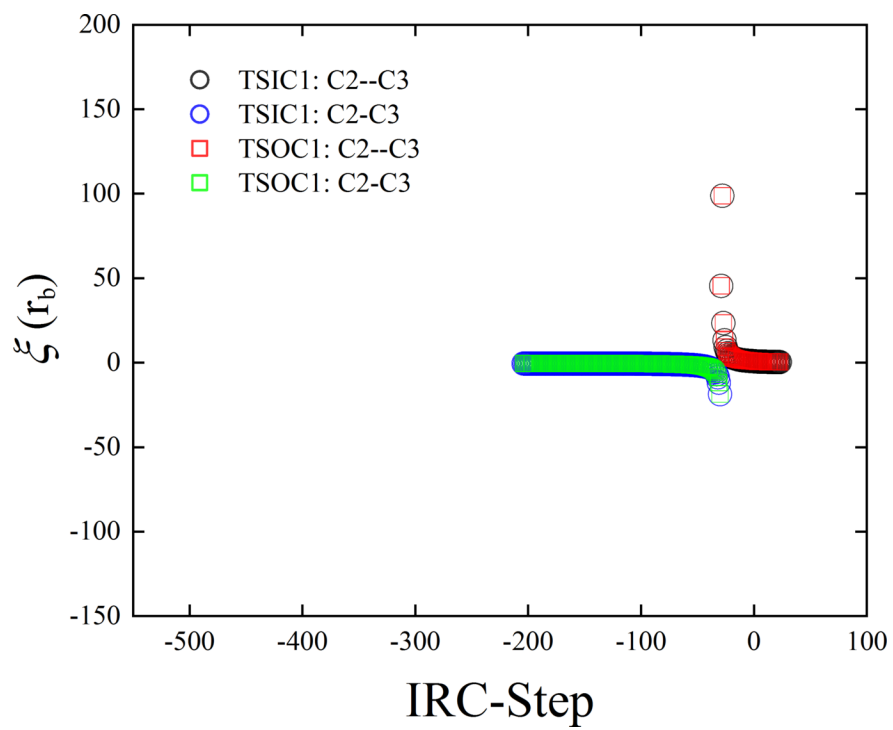
According to what has been discussed in the theory section, the ellipticity ϵ_i values along the bond-paths (r) associated with shared-shell *BCP* s could demonstrate if the bond is a single or double bond character not the same for the closed-shell *BCP* s. This has been done to decide the inclination for either the transition state (TS) outward conrotatory (TSOC) or the transition state inward conrotatory reaction pathway (TSIC). To gain predictions of the TSIC or TSOC product preference, we will analyze the bond paths of the shared-shell ring-opening *BCP* s of the TSIC and TSOC reaction pathways before they alter to closed-shell *BCP* s or rupture completely. Subsequently, the plots of the variation of the bond-path length (BPL) with the IRC for both TSIC and TSOC reactions of the ring-opening C2-C3/C2-C3 *BCP* were evaluated. In addition, the non-degeneracy and degeneracy trend of each reaction shows that Reaction 1 is degenerate while in opposite Reaction 2 , Reaction 3 , and Reaction 4 show significant differences for the corresponding variations and exhibit non-degenerate values. Therefore, in agreement with the QTAIM and stress tensor *BCP* properties, we demonstrate Reaction 1 as a competitive reaction and Reaction 2 , Reaction 3 , and Reaction 4 as non-competitive reactions, see Figures (1-4(i)) respectively. The favored TSIC or TSOC pathway is determined by the greater length H , which is constructed from the e_2 eigenvector tip paths alongside the bond-path (r) for a pair of TSIC and TSOC pathways that are being compared. Larger deviations of the tips are associated with greater deviations of the tips from the original orientation of the e_2 at the *BCP* of TSIC or TSOC pathways. Notice that e_1 and e_2 eigenvectors are associated with the least and most preferred direction of $\rho(r)$ accumulation. As a result, a larger value of H is relating to the most easily distorted molecular graph and accordingly determines the preference for either the TSIC or TSOC pathways. Consequently, we introduce that for the shared-shell ring-opening *BCP* s, greater H lengths predict the preferred TSIC or TSOC reaction pathway. Besides, the variation of the H with the IRC for the TSIC and TSOC for all four reactions were display similar behavior like QTAIM and stress tensor measures that are discussed above. According to the results that obtained from the variation of the H plots, we suggest that Reaction 1 is a competitive reaction and Reaction 2 , Reaction 3 , and Reaction 4 are non-competitive reactions, see Figures (1-4(j)) respectively. However, the helicity length H values demonstrate subtle differences amidst TSIC and TSOC reaction pathways. Consequently, the torquoselectivity preferences of Reaction 2 , Reaction 3 , and Reaction 4 are TSOC, TSOC, and TSIC respectively based on the Longer H values, which is in confirmation with the experimental results shown in Table 1 , Figures (1-4) .



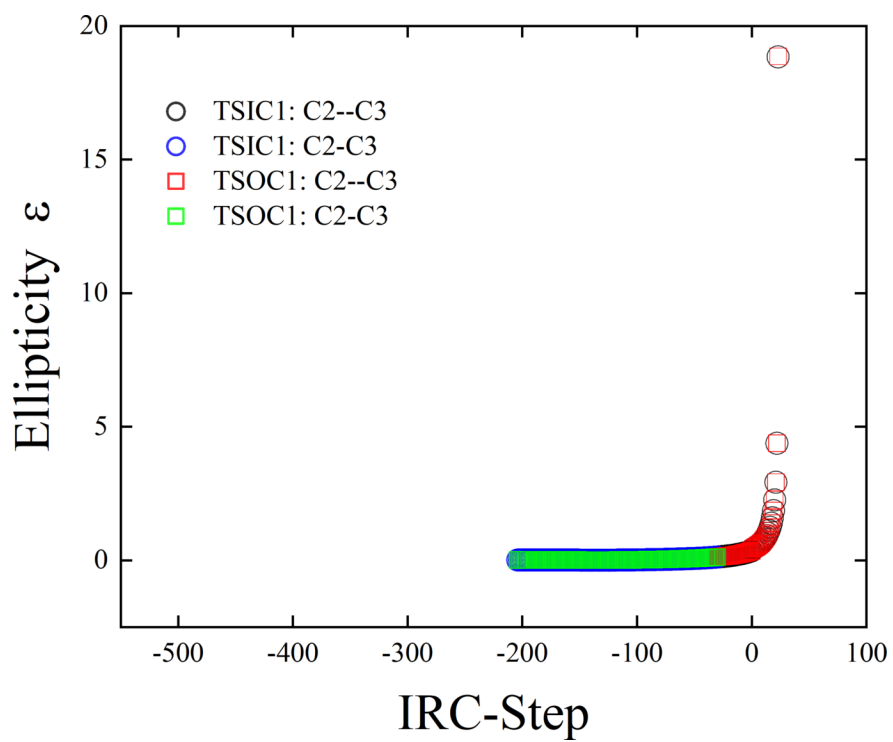
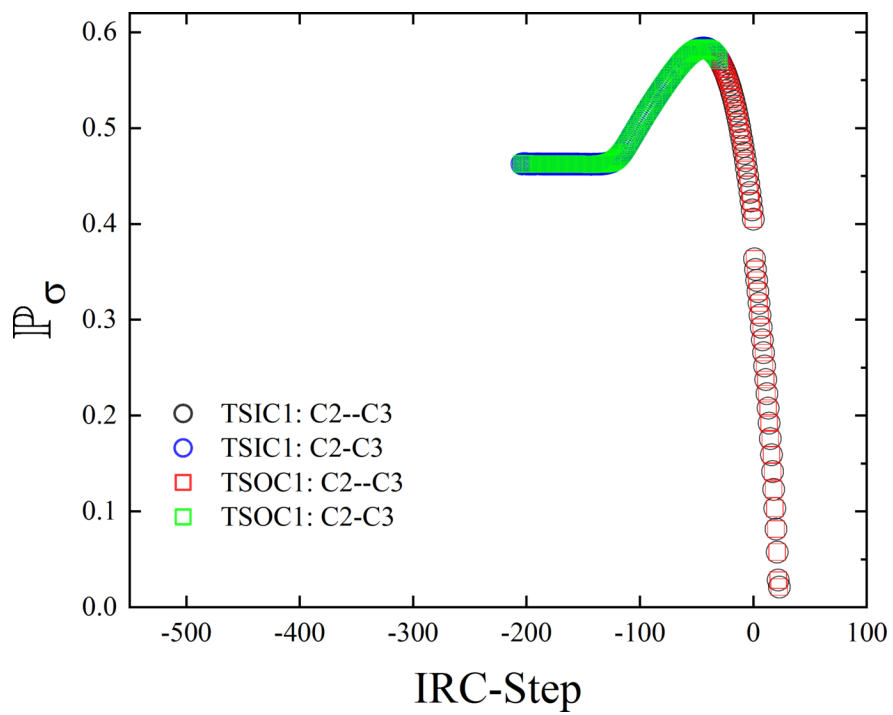


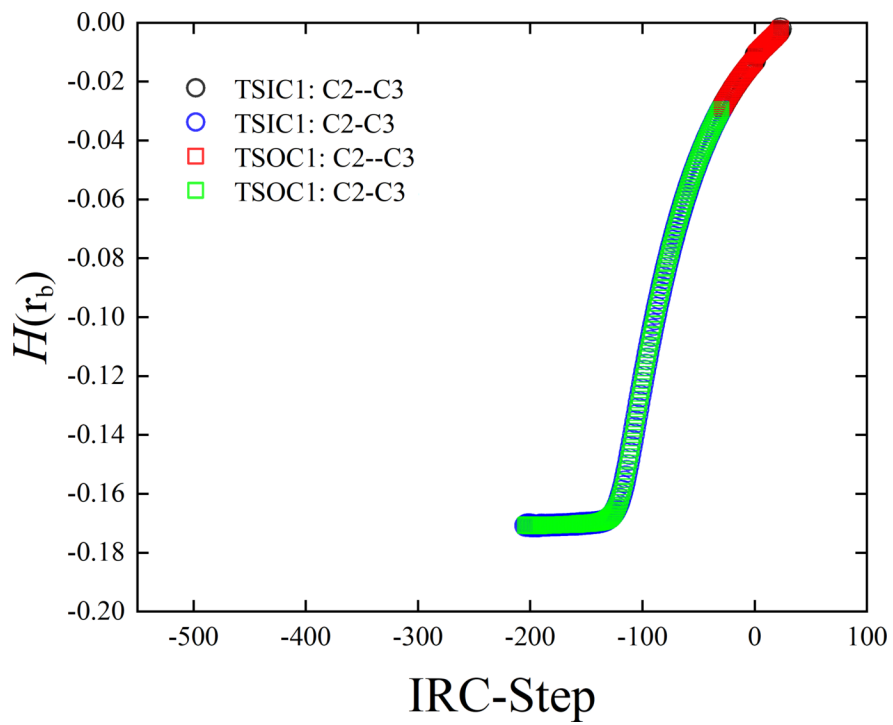


(a) (c) (b)

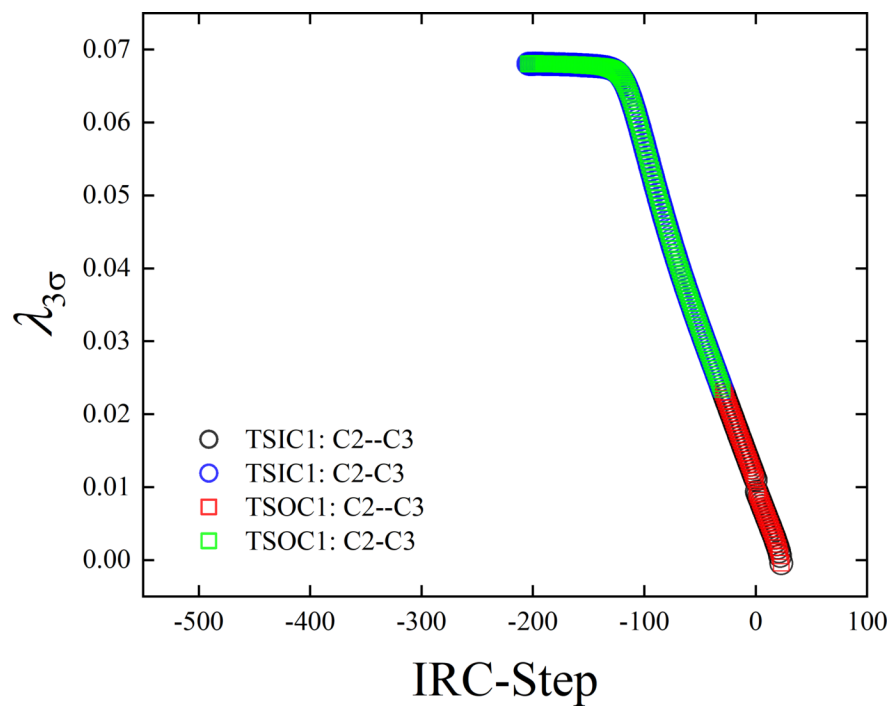


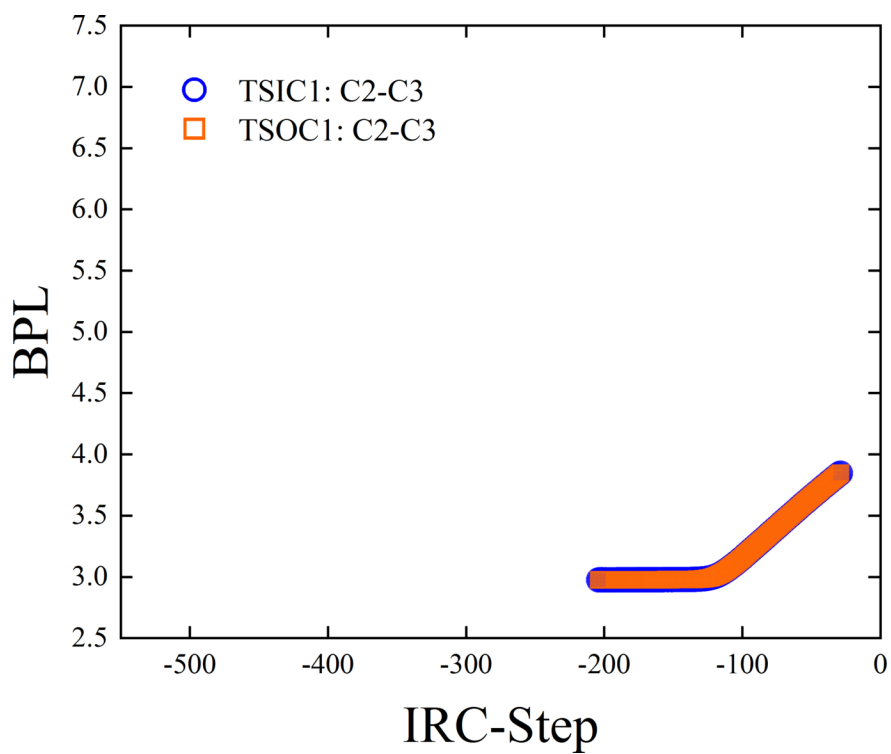
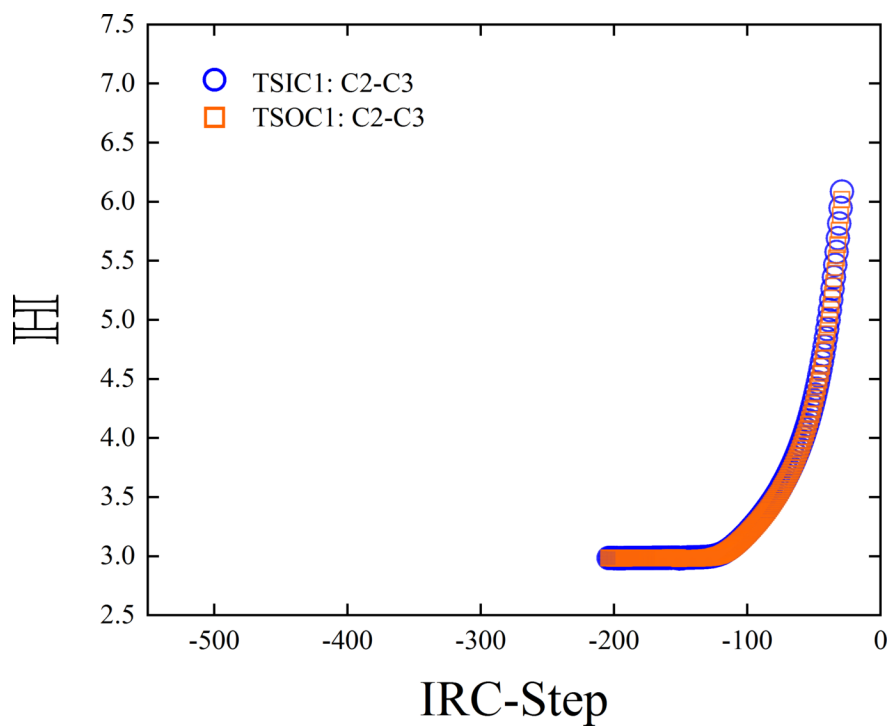
(d)





(e) (f) (g)

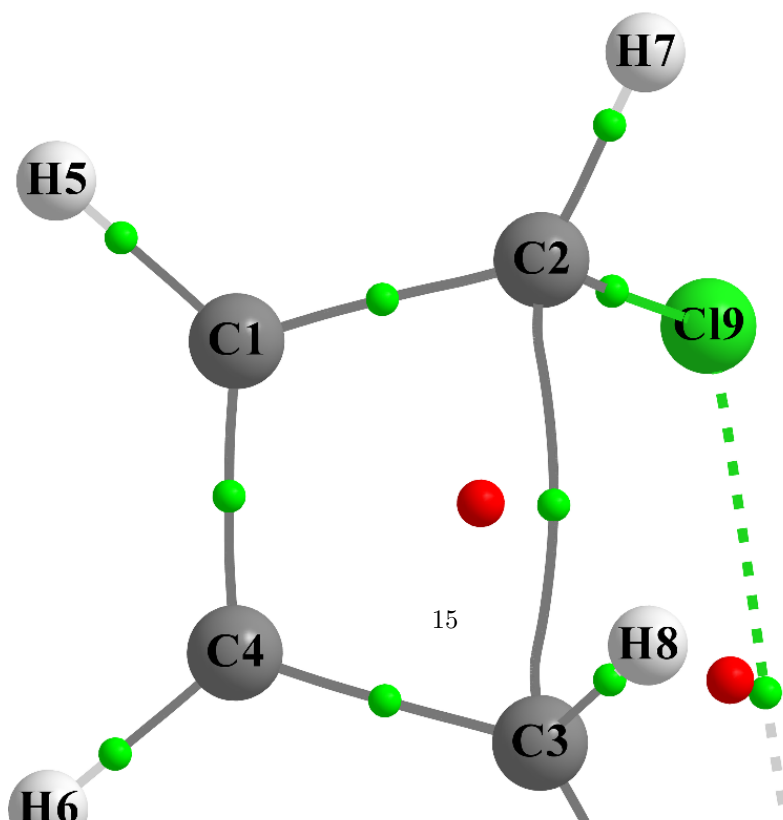
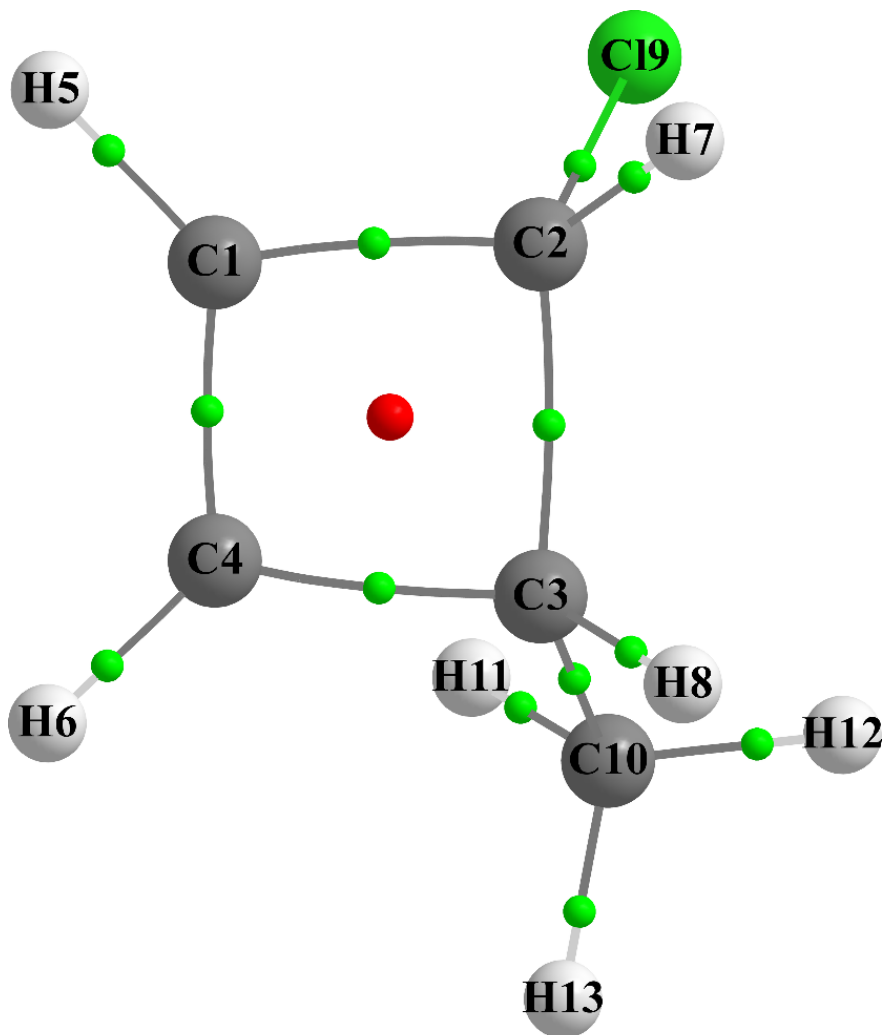


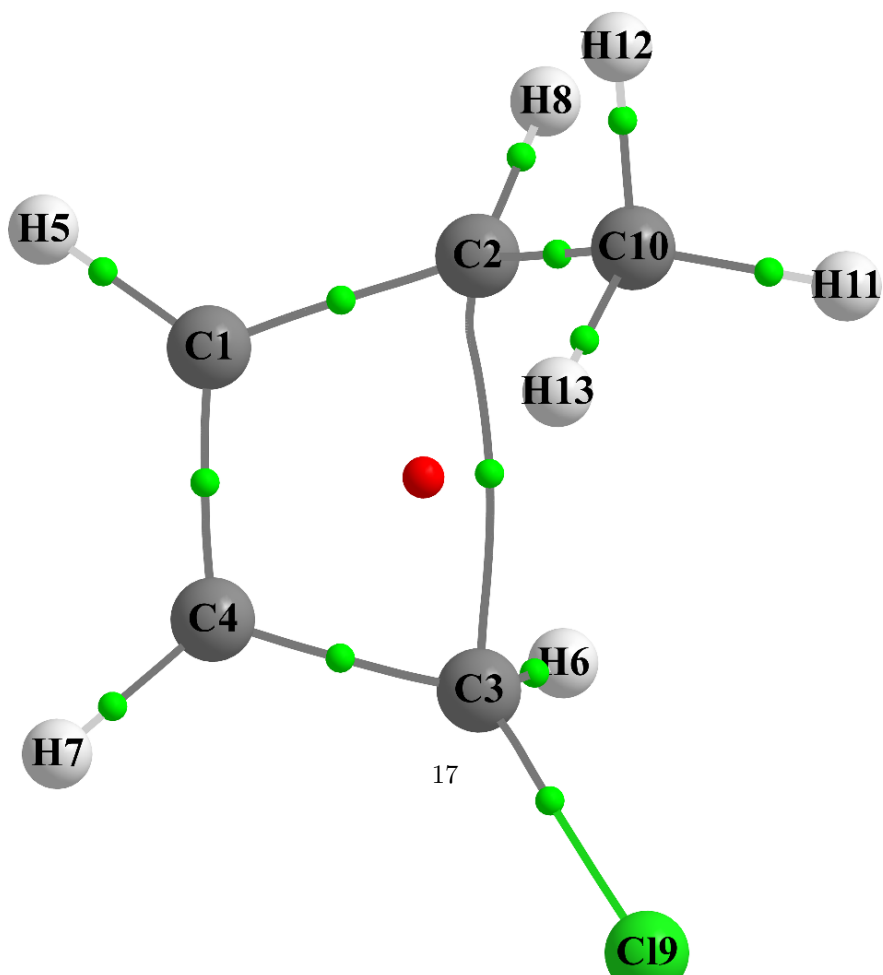
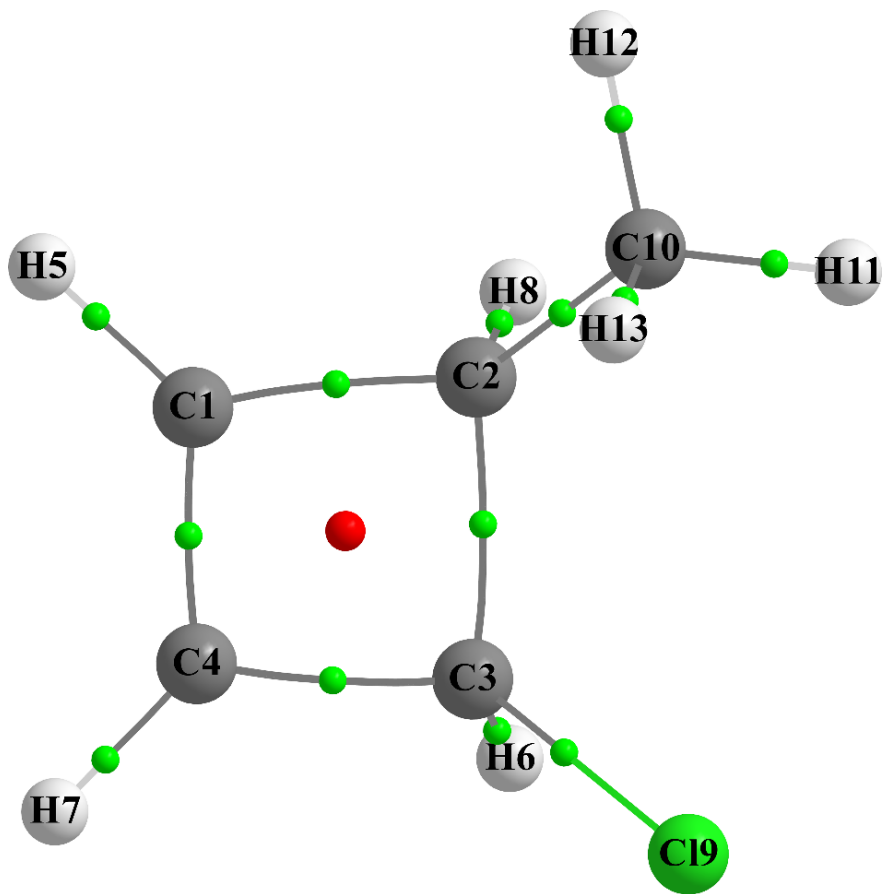


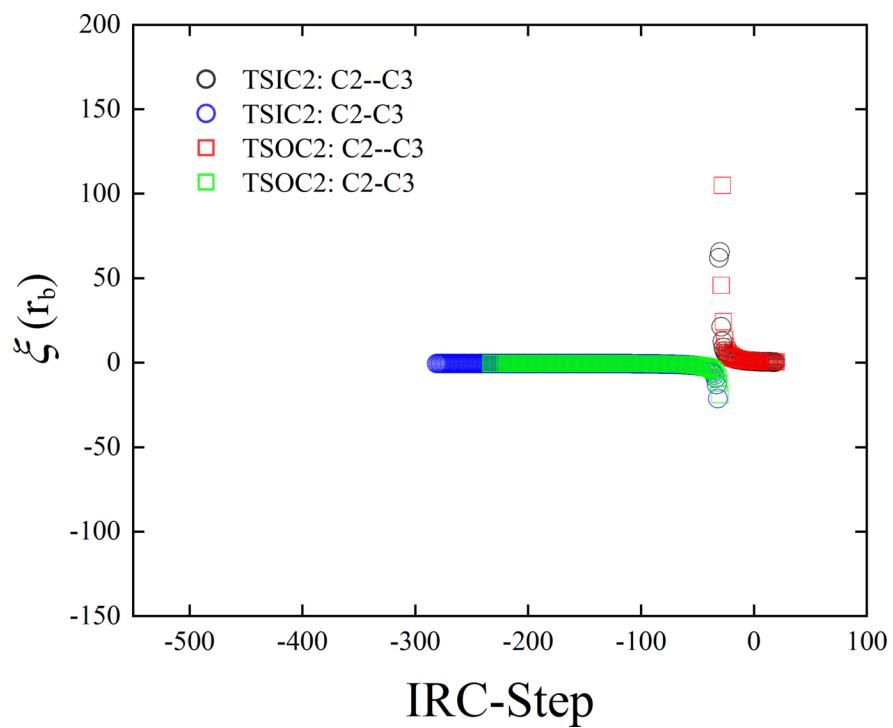
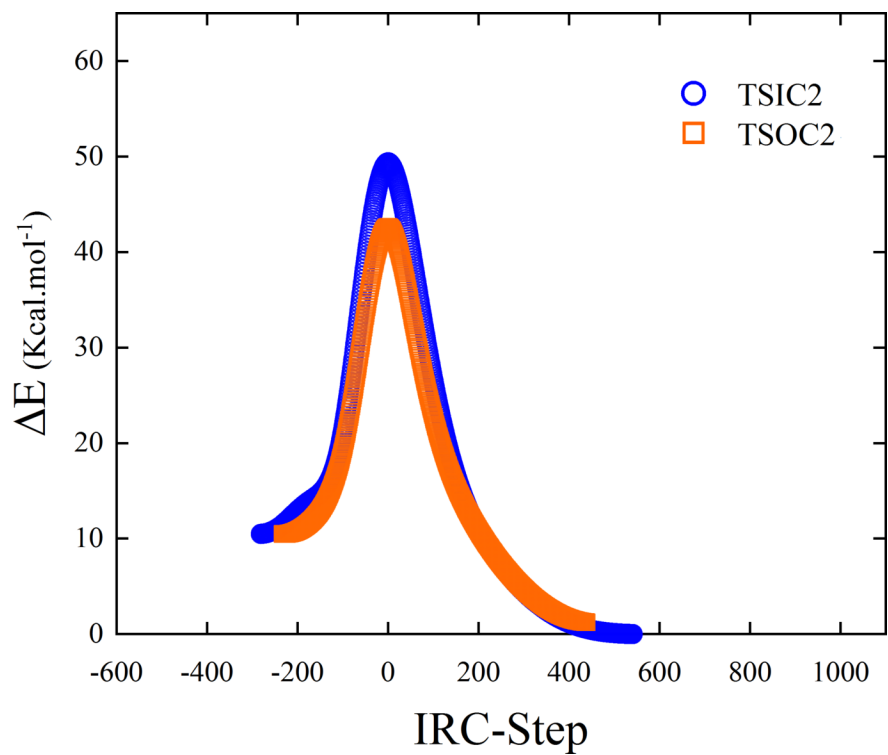
(h) (i) (j)

Figure 1 . Set of bond paths and critical points demonstrate as a molecular graph for the

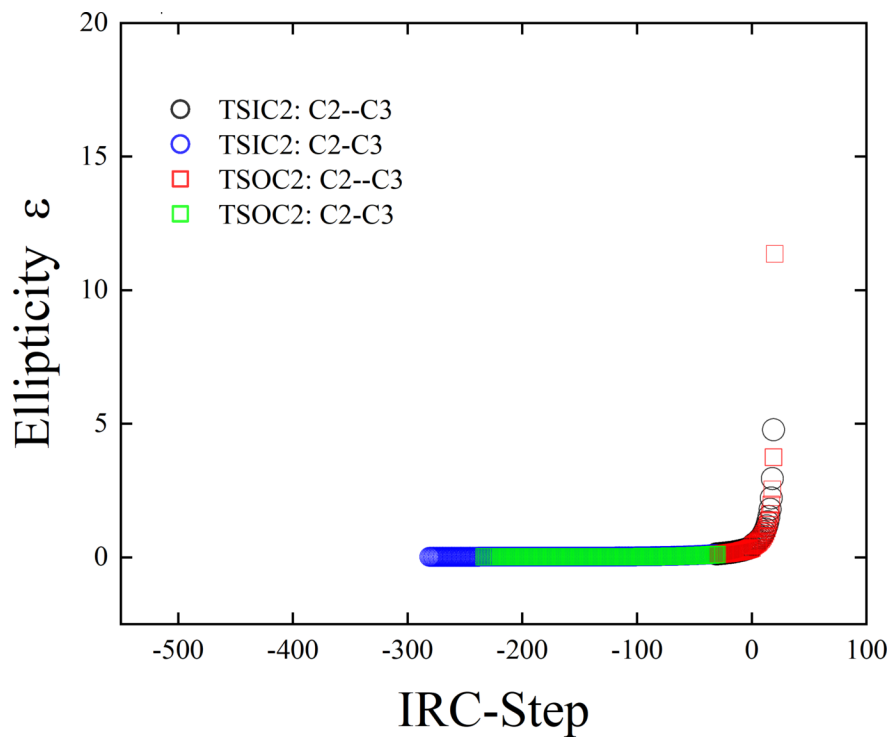
reverse minima, transition state, and forward minima are presented at up, middle, and down panels of the sub-figures(a) and (b) relevant to the outward conrotatory (TSOC) and the inward conrotatory (TSIC) reaction pathways respectively for Reaction 1. Small red and green spheres illustrate the ring critical points (*RCP*s) and bond critical points (*BCP*s) respectively. Where the total local energy $H(r_b)$ of the *BCP*s is more than zero are demonstrated with dashed bond paths. Subfigures (c-j) are illustrated the variation of the relative energy E , metallicity $\xi(r_b)$, ellipticity ϵ , the total local energy density $H(r_b)$, stress tensor polarizability P_σ , stress tensor eigenvalue $\lambda_{3\sigma}$, bond-path length (BPL) and helicity length H along with IRC for Reaction 1 respectively. The alternation from the ring-opening C2-C3 shared-shell *BCP*s to a closed-shell C2-C3 *BCP*s indicates a shift in a sign of the Laplacian $\rho(r_b) < 0$ to $\rho(r_b) > 0$.



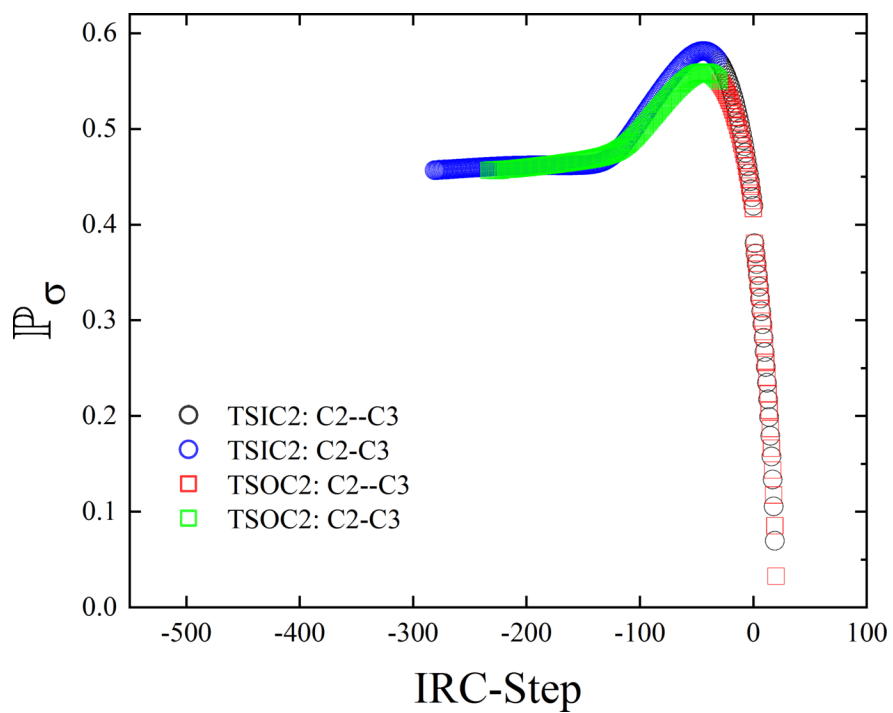


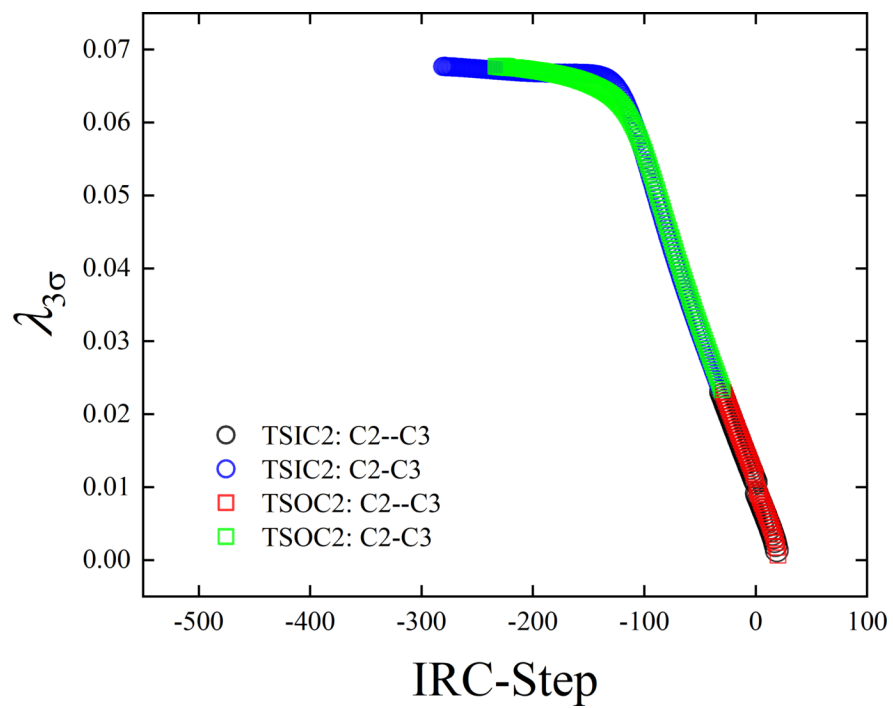
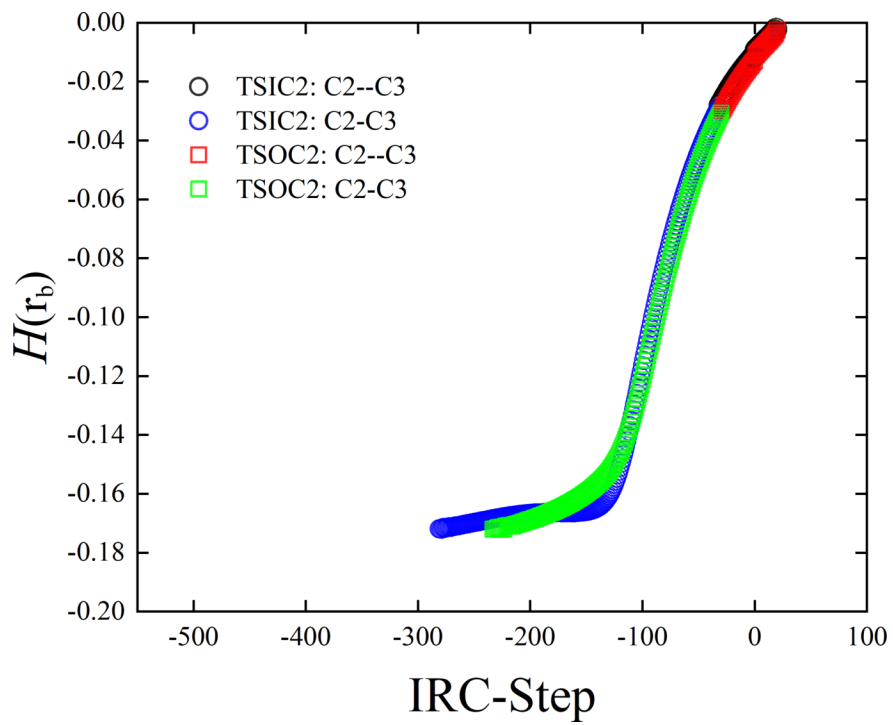


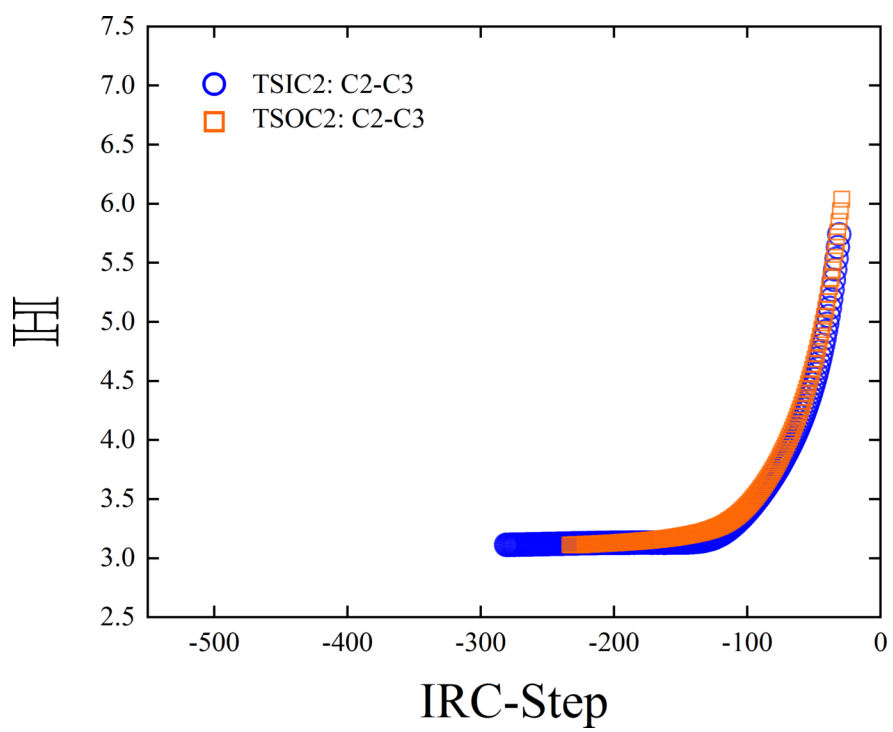
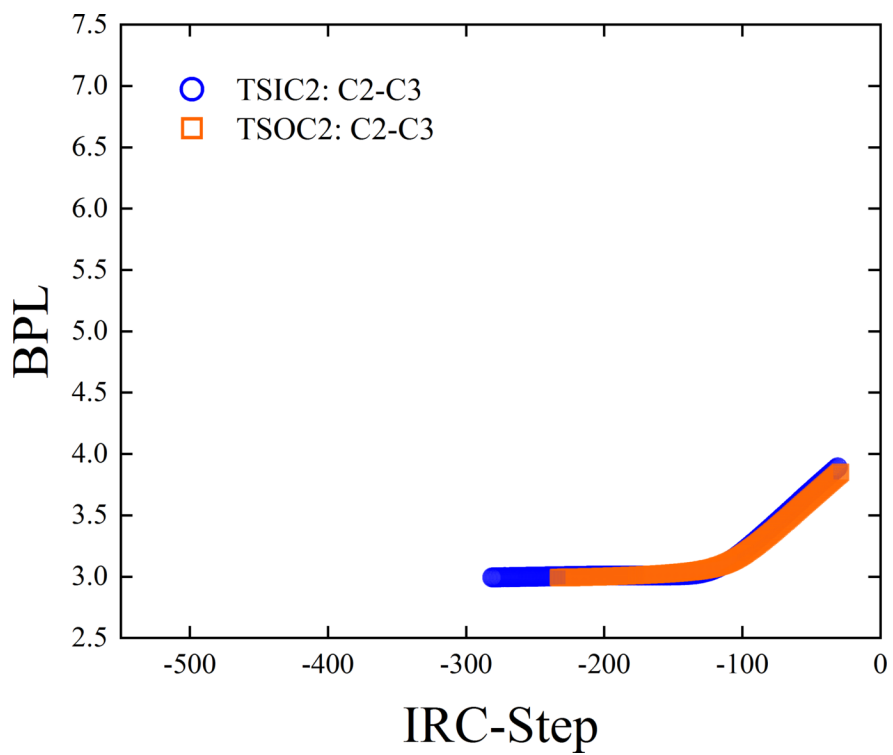
(a) (c) (b)



(d)

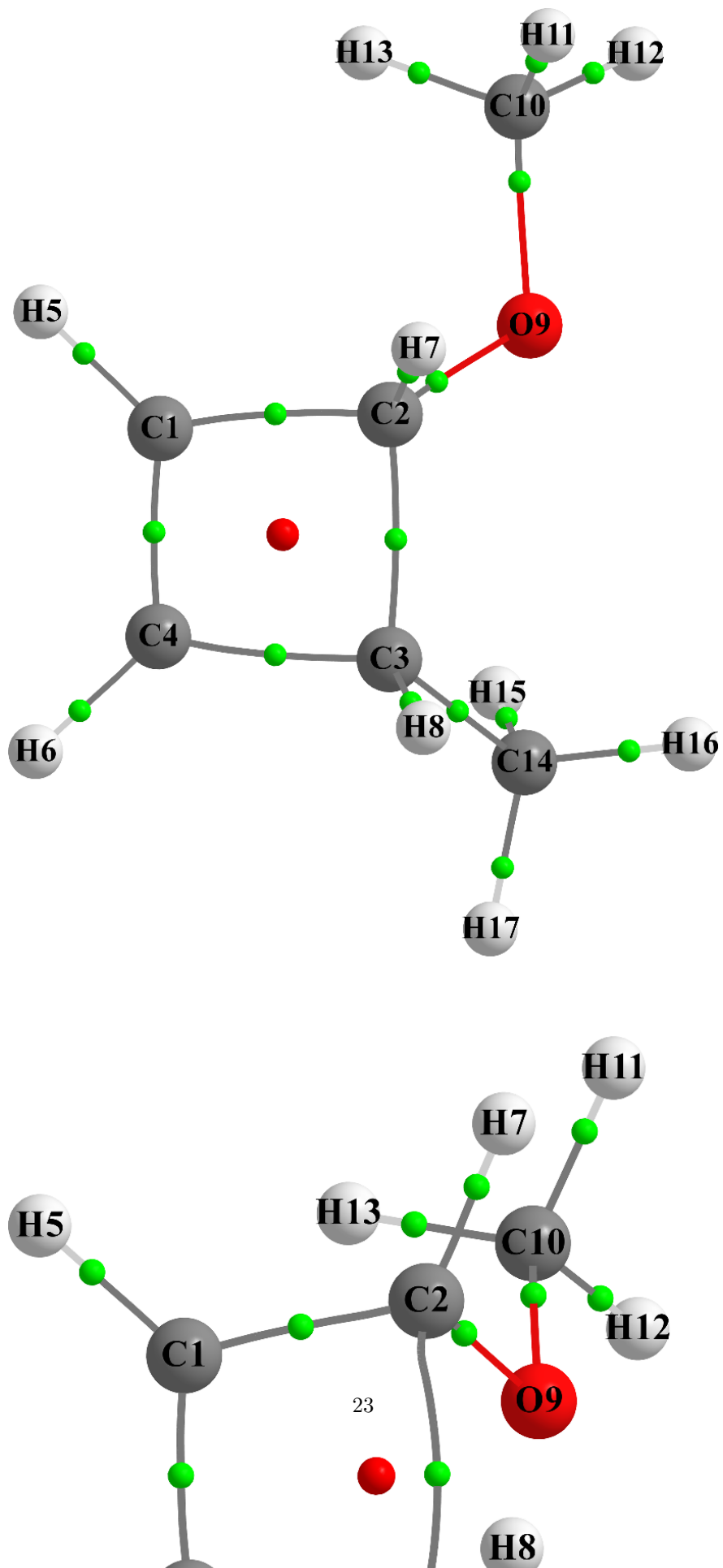


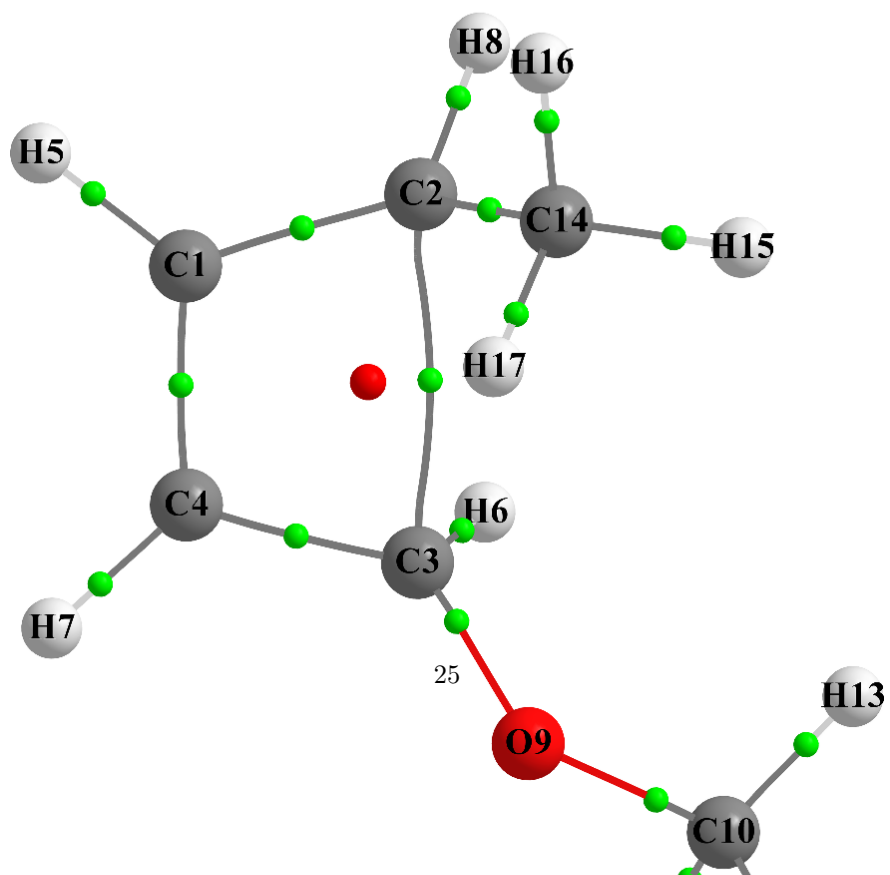
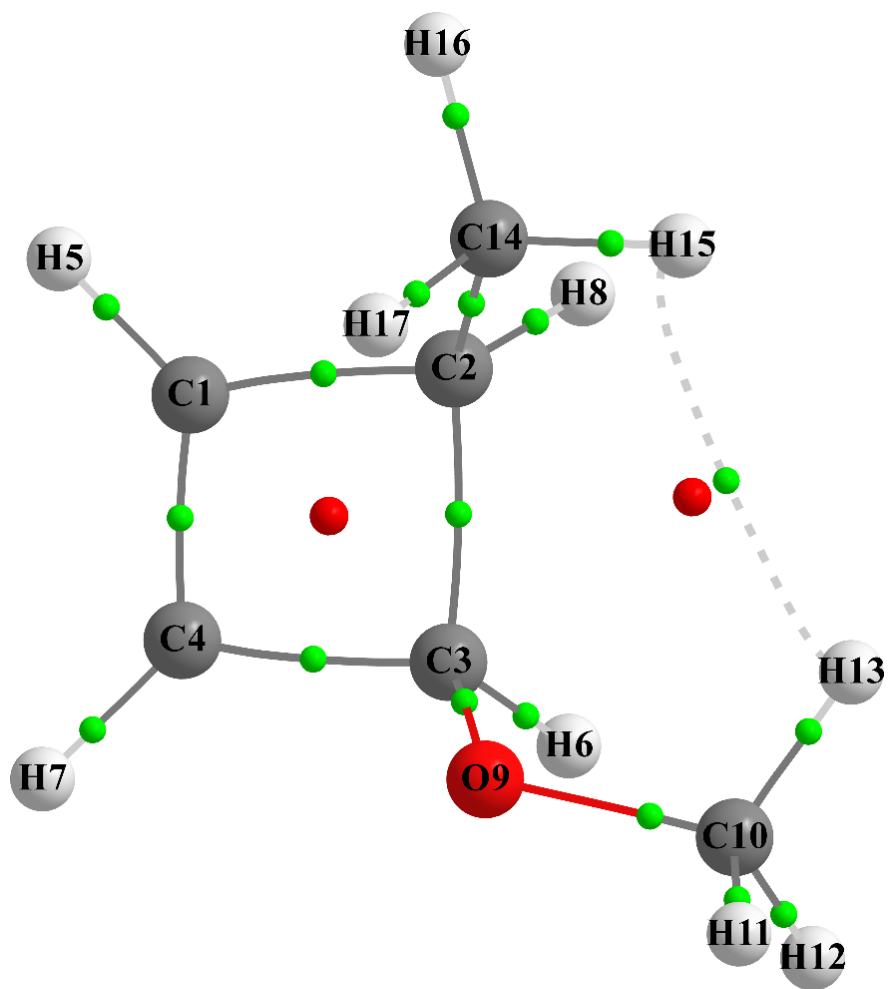


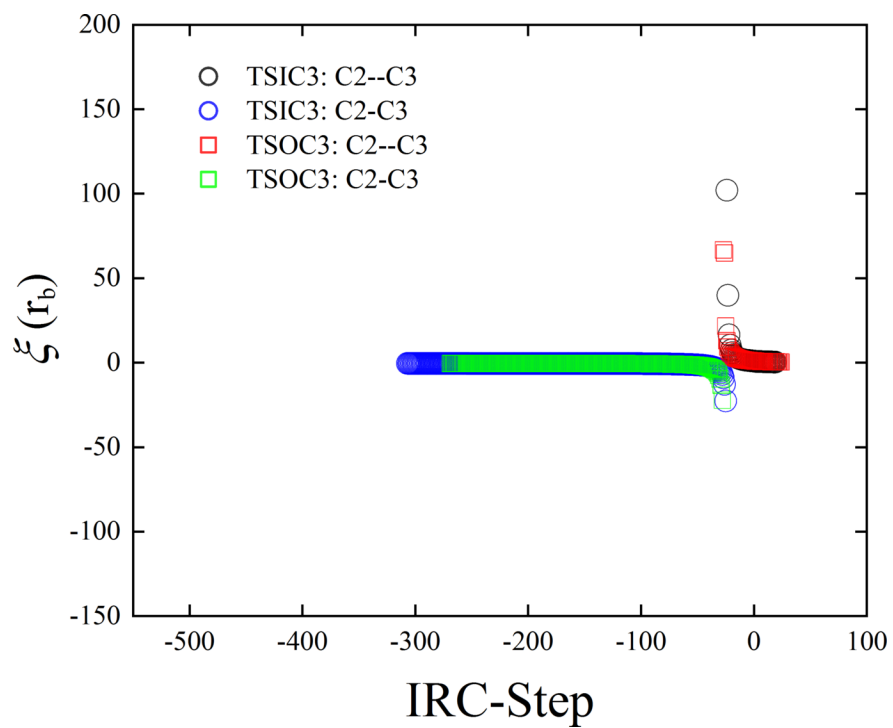
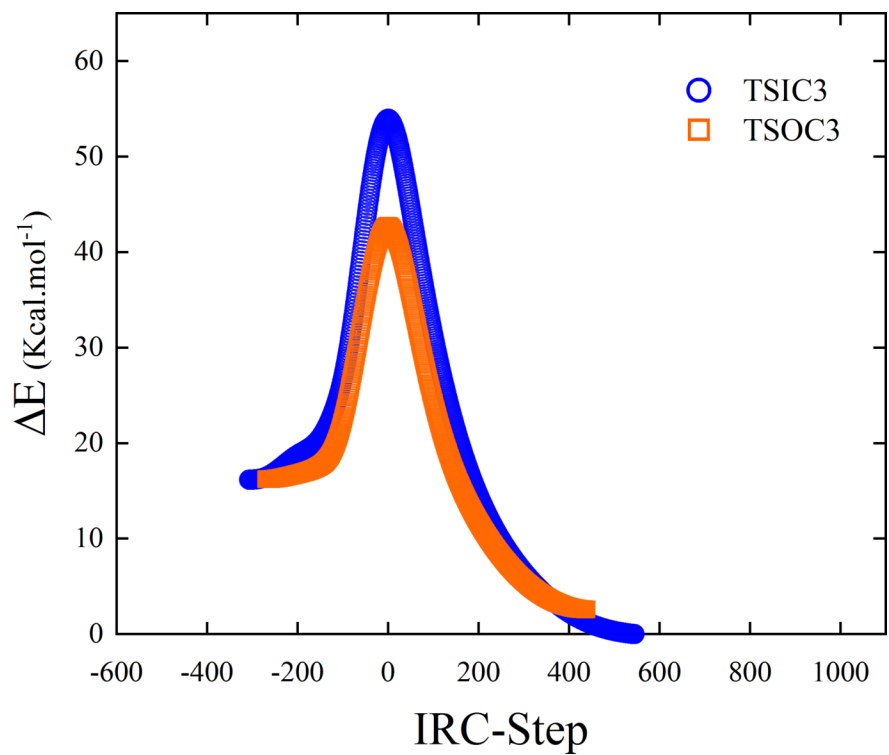


(e) (f) (g)
(h) (i) (j)

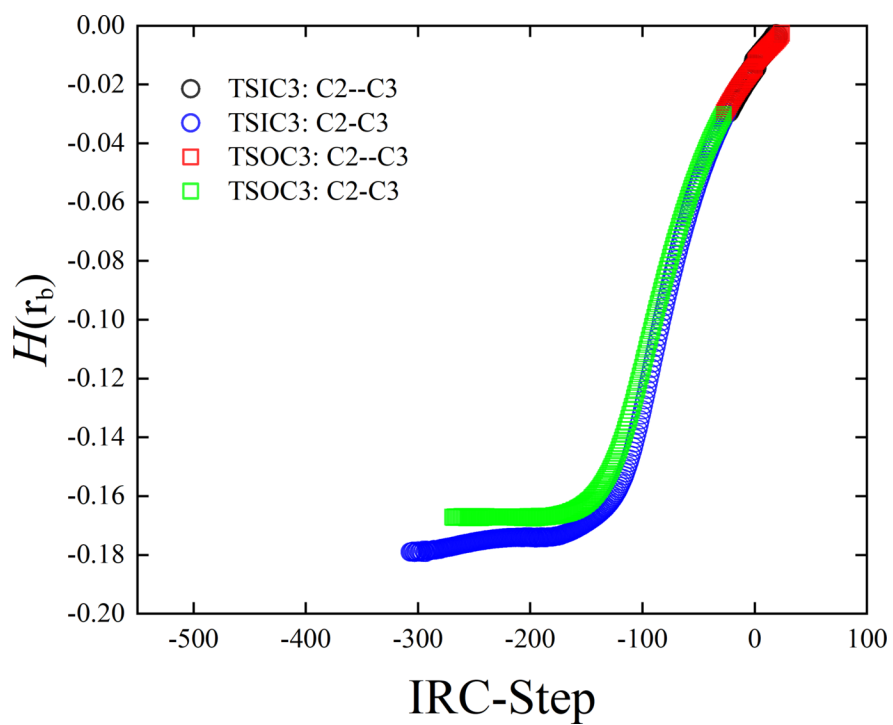
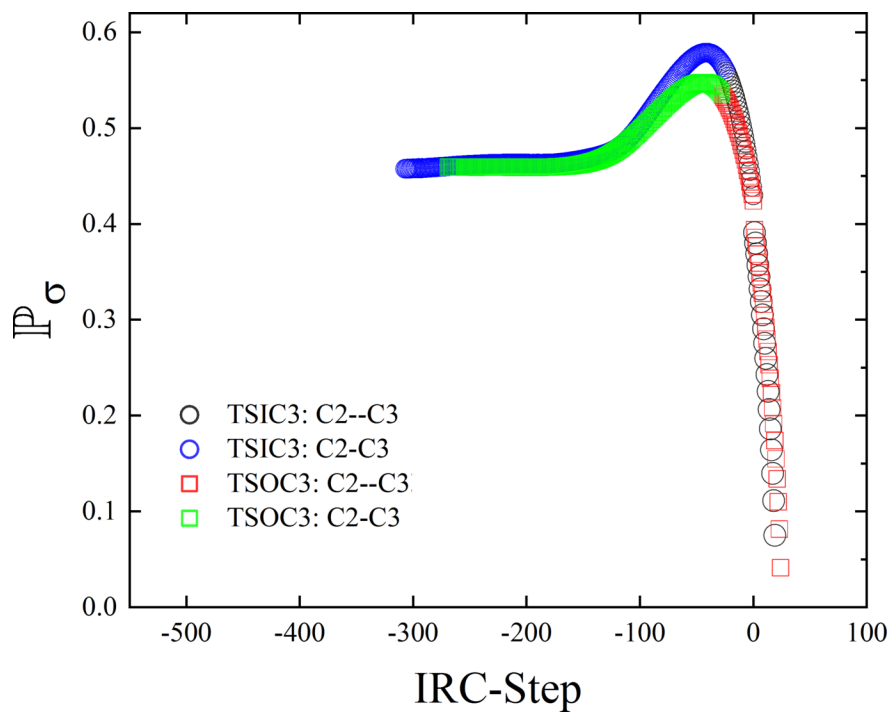
Figure 2 . Snapshots of the molecular graph relevant to the outward conrotatory (TSOC) and the inward conrotatory (TSIC) reaction pathways, the variation of the relative energy $[E]$, metallicity $\xi(r_b)$, ellipticity ϵ , the total local energy density $H(r_b)$, stress tensor polarizability P_σ , stress tensor eigenvalue $\lambda_{3\sigma}$, bond-path length (BPL) and helicity length H along with IRC for Reaction 2 are presented in subfigures(a-j) are respectively. Refer to the caption of Figure 1 for further details.

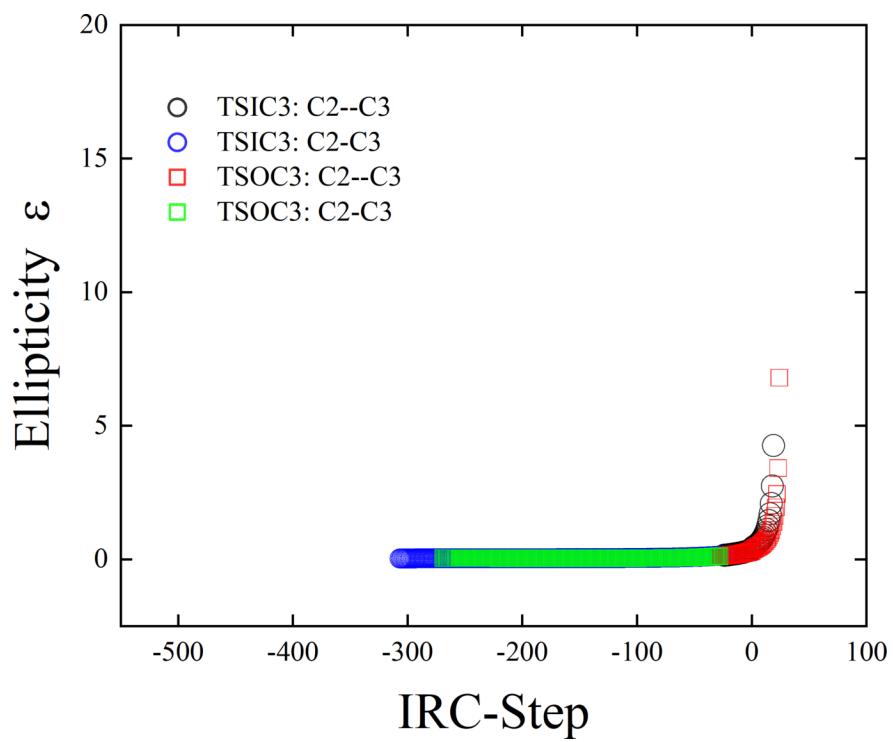






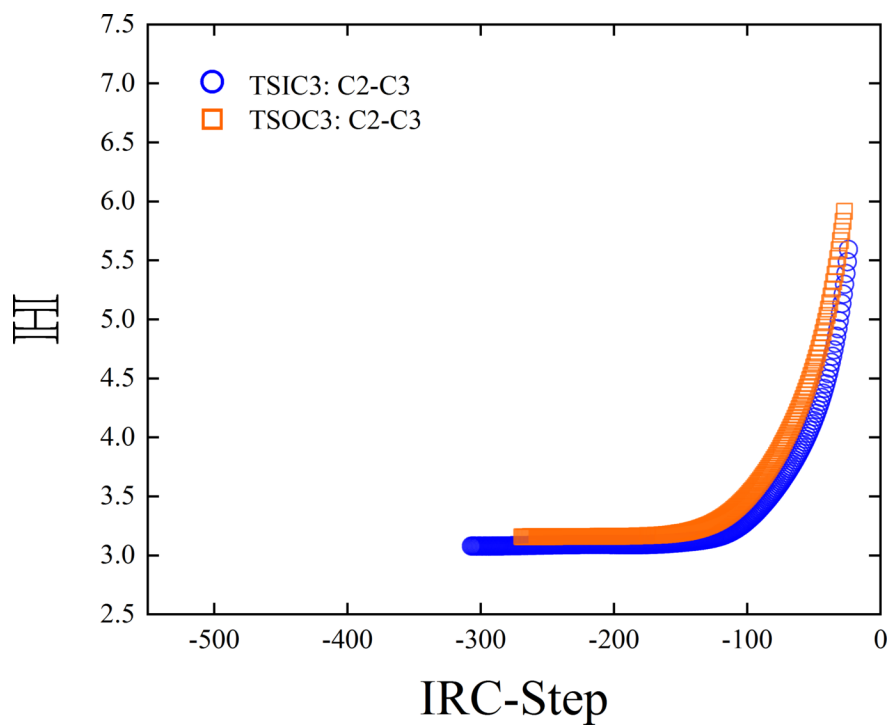
(a) (c) (b)

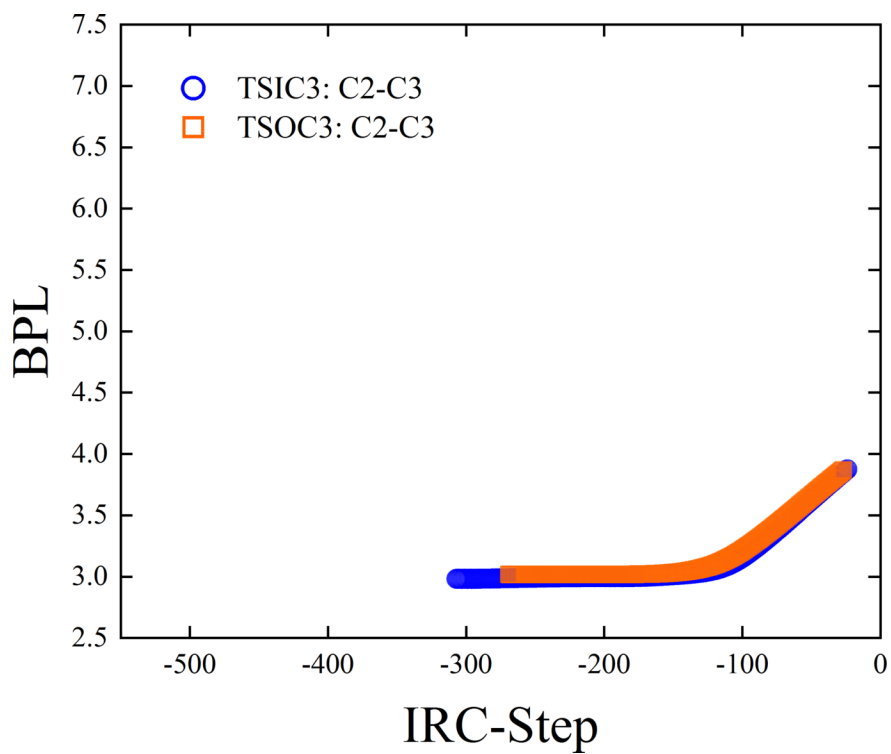
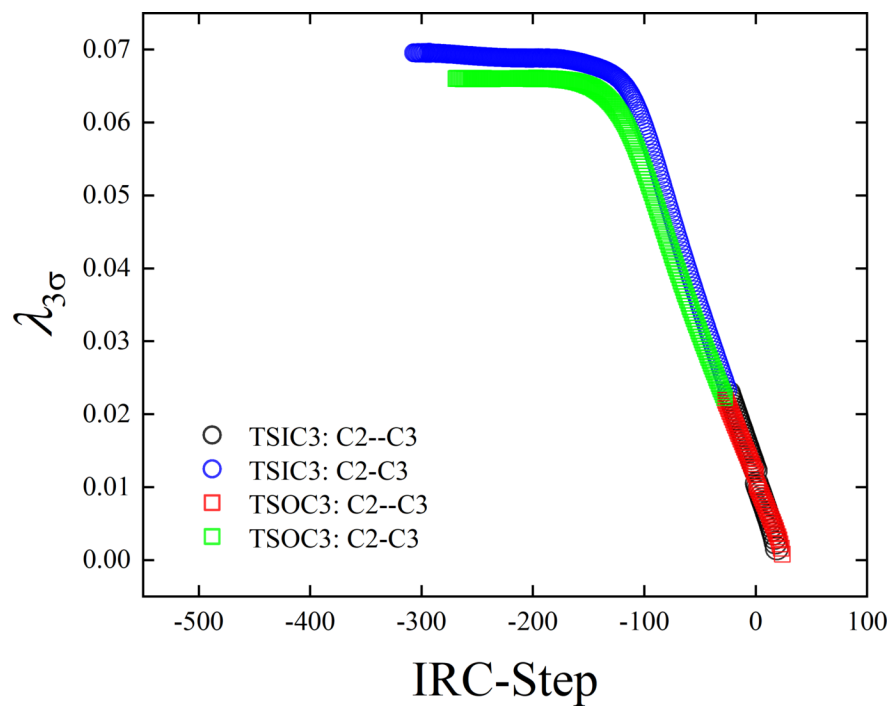




(d)

(e) (f) (g)

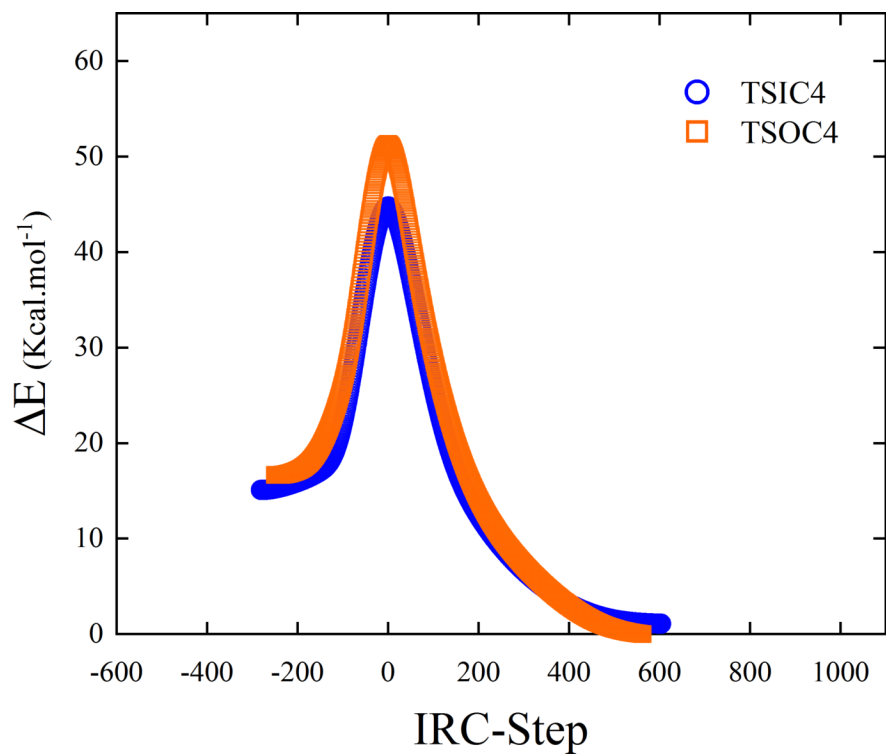


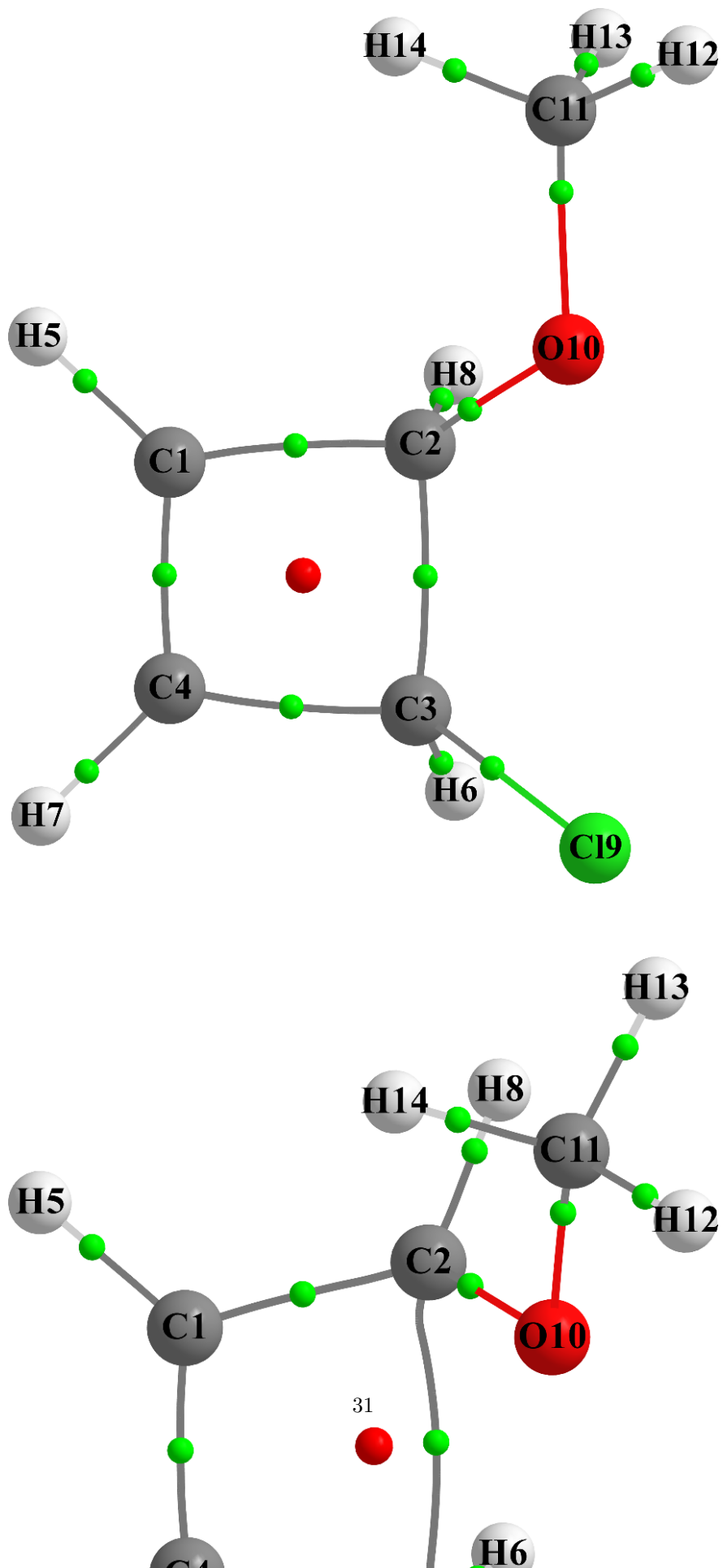


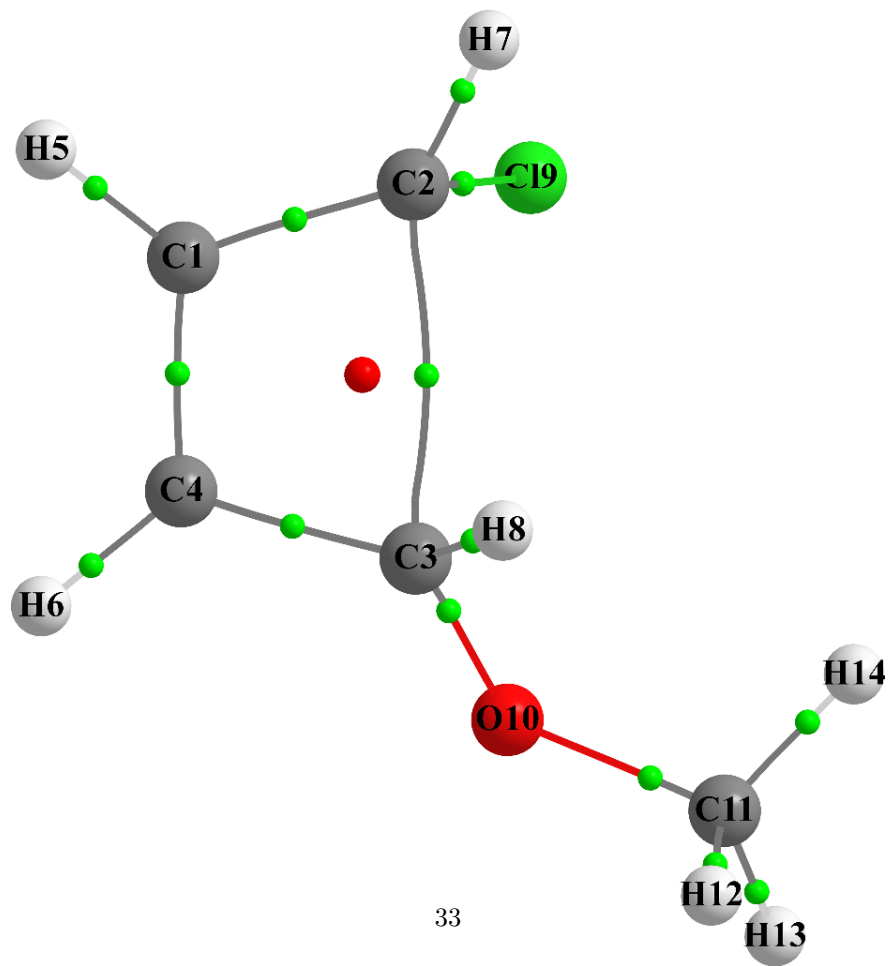
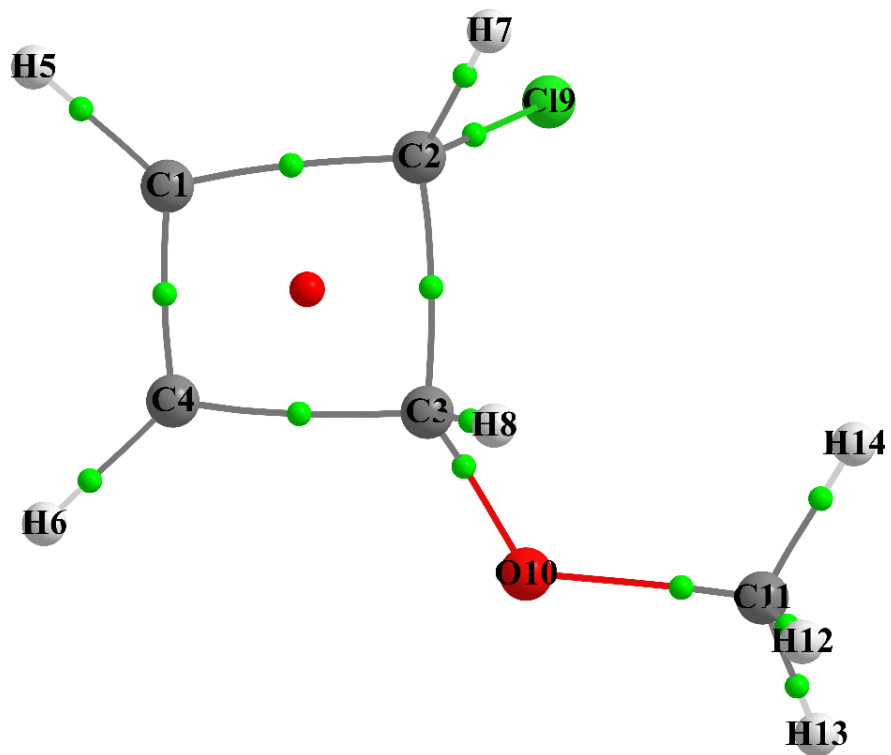
(h) (i) (j)

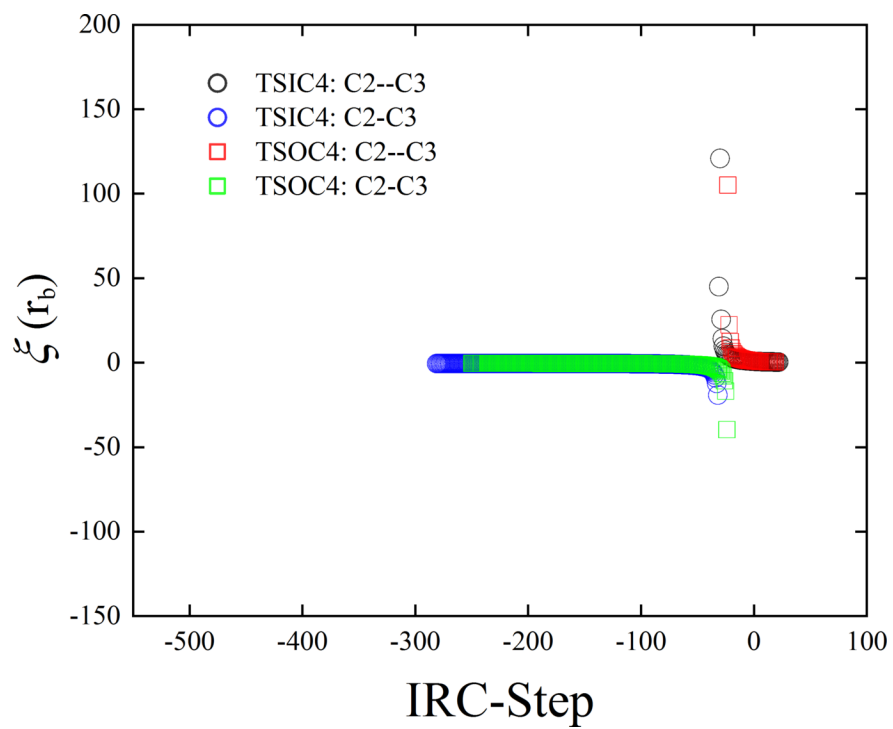
Figure 3 . Snapshots of the molecular graph relevant to the outward conrotatory (TSOC) and the inward conrotatory (TSIC) reaction pathways, the variation of the relative energy

[?] E , metallicity $\xi(r_b)$, ellipticity ϵ , the total local energy density $H(r_b)$, stress tensor polarizability P_σ , stress tensor eigenvalue $\lambda_{3\sigma}$, bond-path length (BPL) and helicity length H along with IRC for Reaction 3 are presented in subfigures(a-j) are respectively. Refer to the caption of Figure 1 for further details.

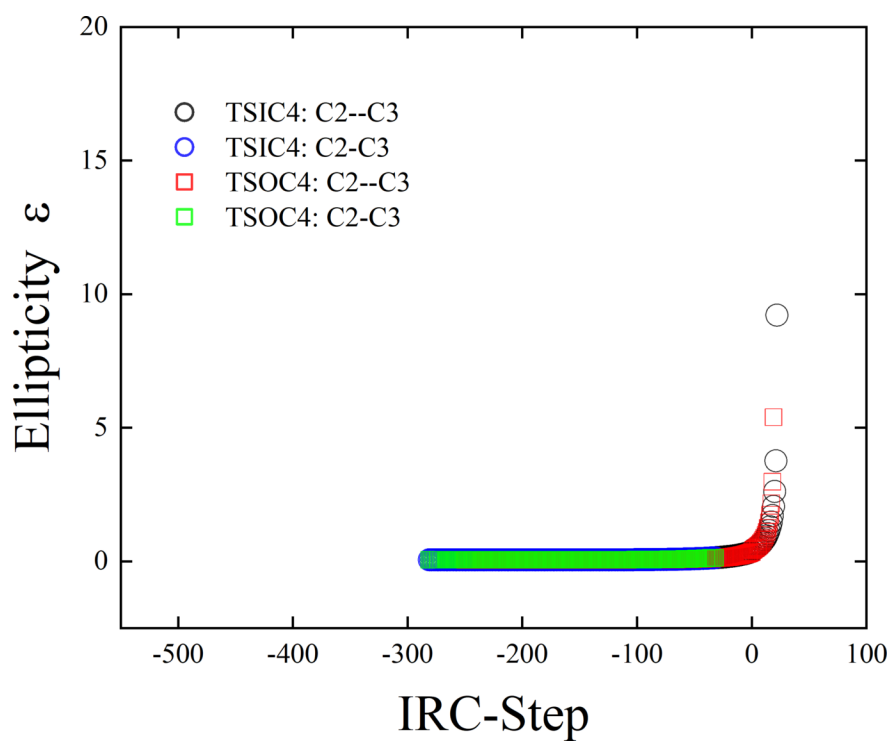




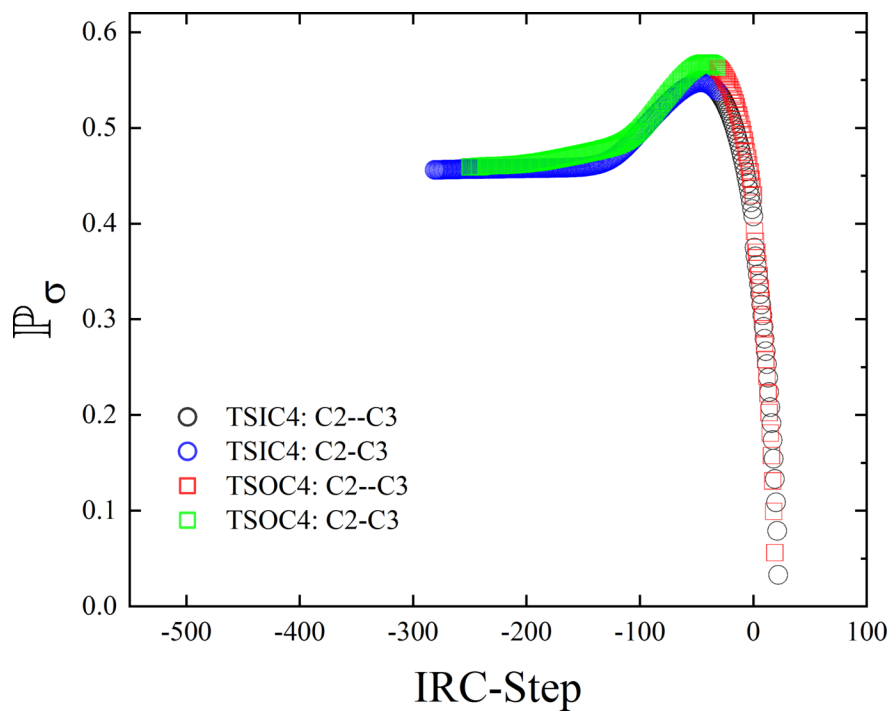
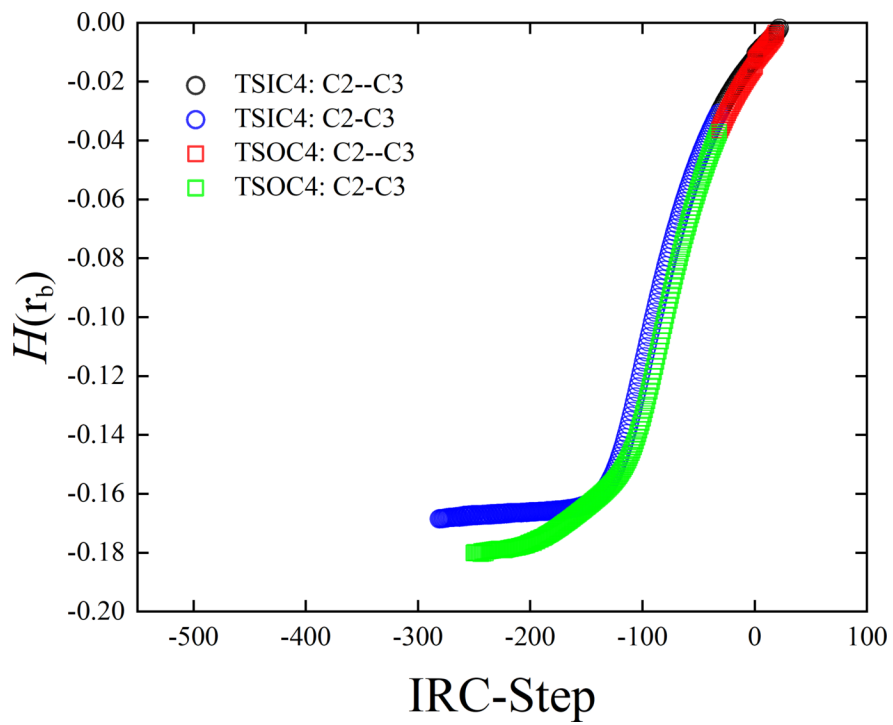


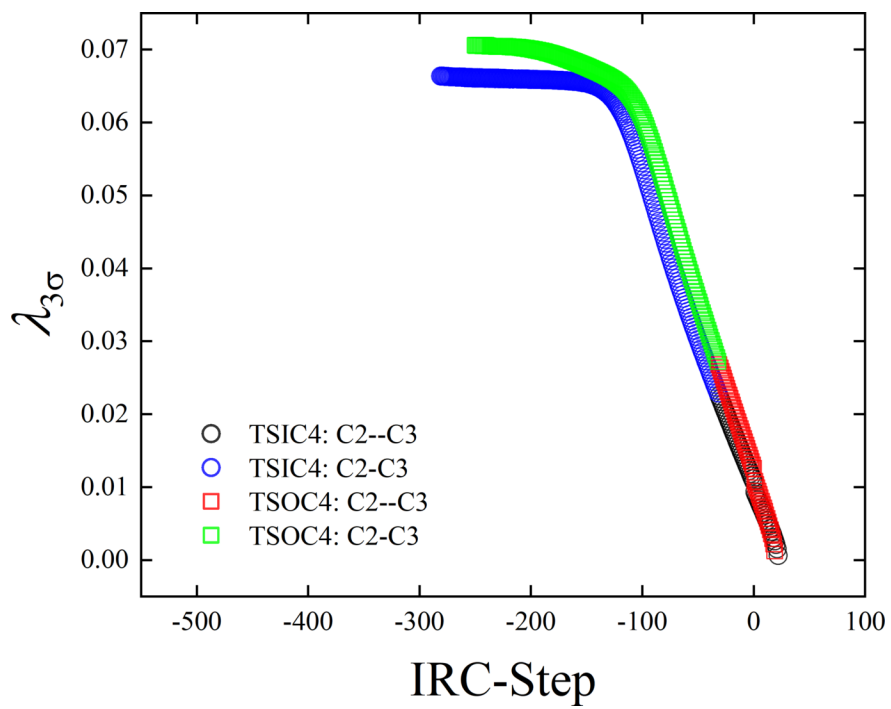


(a) (c) (b)

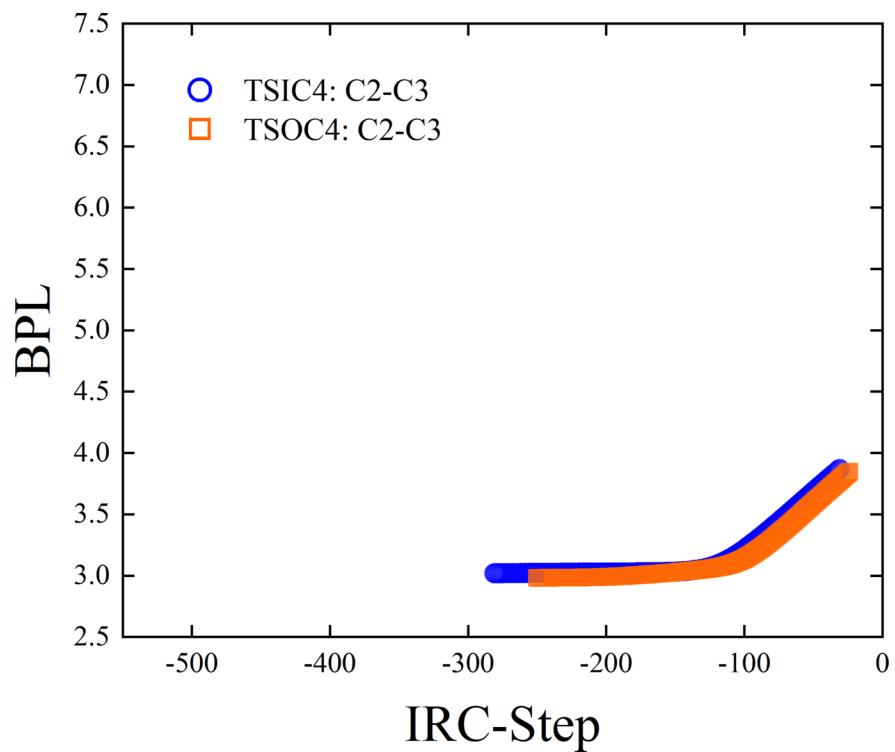


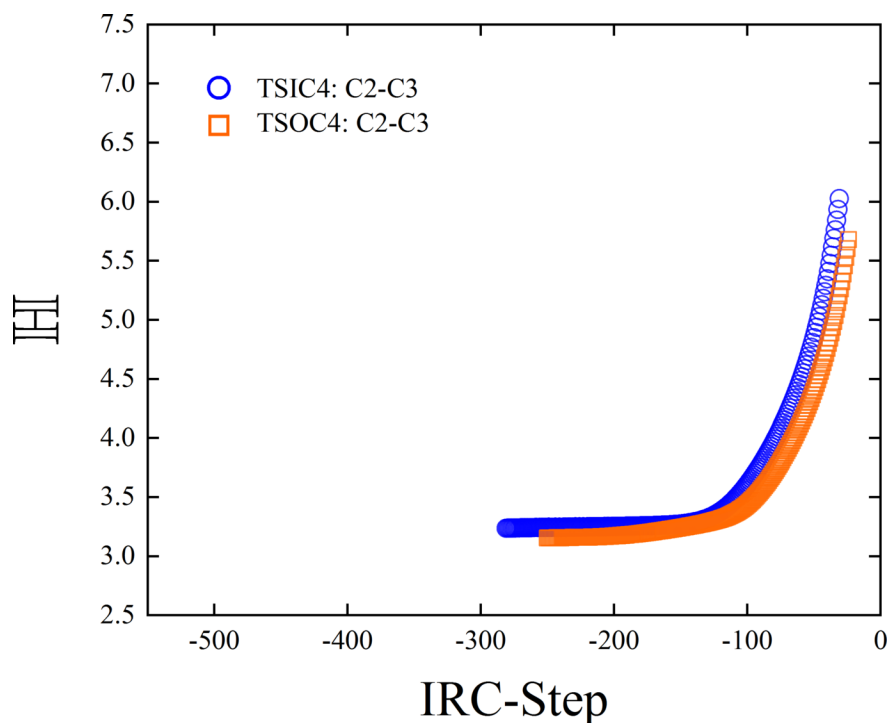
(d)





(e) (f) (g)





(h) (i) (j)

Figure 4 . Snapshots of the molecular graph relevant to the outward conrotatory (TSOC) and the inward conrotatory (TSIC) reaction pathways, the variation of the relative energy $[E]$, metallicity $\xi(r_b)$, ellipticity ε , the total local energy density $H(r_b)$, stress tensor polarizability P_σ , stress tensor eigenvalue $\lambda_{3\sigma}$, bond-path length (BPL) and helicity length H along with IRC for Reaction 4 are presented in subfigures(a-j) are respectively. Refer to the caption of Figure 1 for further details.

5. Conclusions

This investigation represents the study of various non-competitive and competitive reactions utilizing QTAIM and stress tensor analyses. Examination of four reactions in order to distinguish and quantify the TSIC and TSOC paths were performed. In this framework, we have used four disparate cyclobutenes skeleton-based named 1-chlorocyclobut-1-ene, 3-chloro-4-methylcyclobut-1-ene, 3-methoxy-4-methylcyclobut-1-ene, 3-chloro-4-methoxycyclobut-1-ene that identified as Reactions (1-4) respectively. The results from the exploration of QTAIM and stress tensor scalar reveal that each reaction response differently by showing degeneracy or non-degeneracy of the plots. Generally, we conclude that the $\xi(r_b)$ and the P_σ would be useful indicators to predict whether the reaction is competitive or non-competitive following the degeneracy of the results. Overwhelmingly, the determination of these four reactions display that Reaction 1 is a competitive reaction whilst in contrast Reaction 2, Reaction 3, and Reaction 4 are non-competitive reactions. Other stress tensor and QTAIM scalar for instance, the stress tensor eigenvalue $\lambda_{3\sigma}$, the bond-path length (BPL), and the total local energy density $H(r_b)$ also provided the same results in confirmation with metallicity $\xi(r_b)$ and stress tensor polarizability P_σ . Furthermore, illustration of the metallicity $\xi(r_b)$ and stress tensor polarizability P_σ demonstrate that the maximum values and the transition state points do not occur simultaneously in agreement with transition state theory and our previous investigations for other ring-opening (electrocyclic) reactions.

On the other side of this investigation, we used helicity length H with the purpose of predicting the TSIC or TSOC preferences based on data from experiments. Helicity length H plots for non-competitive reactions, Reactions (2-4), could correctly predict the torquoselectivity preferences of either TSIC or TSOC. As a result, that the greater helicity lengths H for shared-shell ring-opening BCP s bond-paths could assist to significantly predict both TSIC or TSOC for these three reactions, Reactions (2-4), exhibit that preference of Reaction 2 is TSOC, Reaction 3 is TSOC, and Reaction 4 is TSIC. The advantage of using H is back to where it is constructed. To make it transparent, e_2 corresponds to the easiest direction or even mention as the most preferred direction, therefore given that H is constructed from a vector representation of the ellipticity ϵ , longer values of H for the TSIC or TSOC would predict the path such as torquoselectivity. The other benefit of the variation of H relevant to the shared-shell ring-opening BCP s bond-paths is that instead of only tracking alternation at the BCP it could track slight changes along the length of the whole ring-opening *bond-path*(r).

Funding Information

This work was financially supported by the National Key Research and Development Program of China (2019YFC1907805).

Acknowledgments

Authors gratefully appreciate Professor Samantha Jenkins and Professor Steven R. Kirk.

References

1. Dolbier William R., H. Koroniak, K. N. Houk and C. Sheu, *Acc. Chem. Res.* , 1996 , 29, 471–477.
2. S. Niwayama, E. A. Kallel, D. C. Spellmeyer, C. Sheu and K. N. Houk, *J. Org. Chem.* , 1996 , 61, 2813–2825.
3. E. A. Kallel and K. N. Houk, *J. Org. Chem.* , 1989 , 54, 6006–6008.
4. D. A. Smith and C. W. Ulmer, *Tetrahedron Letters* ,1991 , 32, 725–728.
5. D. A. Smith and C. W. Ulmer, *J. Org. Chem.* , 1991 , 56, 4444–4447.
6. D. A. Smith and C. W. Ulmer, *J. Org. Chem.* , 1993 , 58, 4118–4121.
7. B. E. T. IV, J. D. Evanseck and K. N. Houk, *Journal of the American Chemical Society* , 1993 , 115, 4165–4169.
8. C. W. Jefford, G. Bernardinelli, Y. Wang, D. C. Spellmeyer, A. Buda and K. N. Houk, *J. Am. Chem. Soc.* , 1992 , 114, 1157–1165.
9. R. Breslow, *Acc. Chem. Res.* , 2004 , 37, 471–478.
10. O. Geßner, A. M. D. Lee, J. P. Shaffer, H. Reisler, S. V. Levchenko, A. I. Krylov, J. G. Underwood, H. Shi, A. L. L. East, D. M. Wardlaw, E. t H. Chrysostom, C. C. Hayden and A. Stolow, *Science* ,2006 , 311, 219–222.
11. B. T. Sutcliffe, *Molecular Physics* , 2006 , 104, 715–722.
12. K. Fukui, *J. Phys. Chem.* , 1970 , 74, 4161–4163.
13. R. S. Mulliken, *J. Chem. Phys.* , 1955 , 23, 1833–1840.
14. A. E. Reed, L. A. Curtiss and F. Weinhold, *Chem. Rev.* ,1988 , 88, 899–926.
15. R. F. W. Bader, *Atoms in Molecule: A Quantum Theory* ,1990 , vol. 22.

16. S. Grimme, C. Mück-Lichtenfeld, G. Erker, G. Kehr, H. Wang, H. Beckers and H. Willner, *Angewandte Chemie International Edition* ,2009 , 48, 2592–2595.
17. A. D. Becke and K. E. Edgecombe, *J. Chem. Phys.* ,1990 , 92, 5397–5403.
18. A. Savin, O. Jepsen, J. Flad, O. K. Andersen, H. Preuss and H. G. von Schnering, *Angewandte Chemie International Edition in English* , 1992 , 31, 187–188.
19. X. KROKIDIS, R. VUILLEUMIER, D. BORGIS and B. SILVI, *Molecular Physics* , 1999 , 96, 265–273.
20. X. Li, Y. Zeng, L. Meng and S. Zheng, *J. Phys. Chem. A* ,2007 , 111, 1530–1535.
21. S. Berski, J. Andrés, B. Silvi and L. R. Domingo, *J. Phys. Chem. A* , 2003 , 107, 6014–6024.
22. L. R. Domingo, M. José Aurell, P. Pérez and R. Contreras, *J. Org. Chem.* , 2003 , 68, 3884–3890.
23. K. N. Houk, J. Gonzalez and Y. Li, *Acc. Chem. Res* ,1995 , 28, 81–90.
24. R. B. Woodward and R. Hoffmann, *Angewandte Chemie International Edition in English* , 1969 , 8, 781–853.
25. A. Morales-Bayuelo, *International Journal of Quantum Chemistry* , 2013 , 113, 1534–1543.
26. A. Morales-Bayuelo and J. Sánchez-Márquez, *Heliyon* ,2020 , 6, e04441.
27. A. Morales-Bayuelo, S. Pan, J. Caballero and P. K. Chattaraj,*Phys. Chem. Chem. Phys.* , 2015 , 17, 23104–23111.
28. H. Guo, A. Morales-Bayuelo, T. Xu, R. Momen, L. Wang, P. Yang, S. R. Kirk and S. Jenkins, *Journal of Computational Chemistry* ,2016 , 37, 2722–2733.
29. A. Morales-Bayuelo, J. Sánchez-Márquez, G. Jana and P. K. Chattaraj,*International Journal of Quantum Chemistry* , 2018 , 118, e25778.
30. A. Morales-Bayuelo, J. Sánchez-Márquez, G. Jana and P. K. Chattaraj,*Struct Chem* , 2020 , 31, 1745–1756.
31. W. R. D. Jr, H. Koroniak, D. J. Burton, A. R. Bailey, G. S. Shaw and S. W. Hansen, *J. Am. Chem. Soc.* , 1984 , 106, 1871–1872.
32. H. M. Frey, *Trans. Faraday Soc.* , 1962 , 58, 957–960.
33. R. F. W. Bader, *Atoms in Molecules: A Quantum Theory* , Oxford University Press, USA, 1994 .
34. R. F. W. Bader, *J. Phys. Chem. A* , 1998 , 102, 7314–7323.
35. R. F. W. Bader, *J. Phys. Chem. A* , 2009 , 113, 10391–10396.
36. S. Jenkins, *J. Phys.: Condens. Matter* , 2002 , 14, 10251–10263.
37. S. Jenkins, P. W. Ayers, S. R. Kirk, P. Mori-Sánchez and A. Martín Pendás, *Chemical Physics Letters* , 2009 , 471, 174–177.
38. B. Herrera and A. Toro-Labbé, *J. Phys. Chem. A* ,2007 , 111, 5921–5926.
39. P. W. Ayers and S. Jenkins, *Computational and Theoretical Chemistry* , 2015 , 1053, 112–122.
40. E. Kraka and D. Cremer, *Journal of Molecular Structure: THEOCHEM* , 1992 , 255, 189–206.

41. S. Jenkins, L. Blancafort, S. R. Kirk and M. J. Bearpark, *Phys. Chem. Chem. Phys.* , 2014 , 16, 7115–7126.
42. Y. Xu, T. Xu, D. Jiajun, S. R. Kirk and S. Jenkins, *Int. J. Quantum Chem.* , 2016 , 116, 1025–1039.
43. R. F. W. Bader, *The Journal of Chemical Physics* ,1980 , 73, 2871–2883.
44. R. F. W. Bader and T. T. Nguyen-Dang, in *Advances in Quantum Chemistry* , ed. P.-O. Löwdin, Academic Press, 1981 , vol. 14, pp. 63–124.
45. S. Jenkins and M. I. Heggie, *J. Phys.: Condens. Matter* ,2000 , 12, 10325.
46. S. Jenkins and I. Morrison, *Chemical Physics Letters* ,2000 , 317, 97–102.
47. S. Jenkins, *Int. J. Quantum Chem.* , 2013 , 113, 1603–1608.
48. A. Azizi, R. Momen, A. Morales-Bayuelo, T. Xu, S. R. Kirk and S. Jenkins, *International Journal of Quantum Chemistry* ,2018 , 118, e25707.
49. Michael J. Frisch, G. W. Trucks, H. Bernhard Schlegel, Gustavo E. Scuseria, Michael A. Robb, James R. Cheeseman, Giovanni Scalmani, Vincenzo Barone, Benedetta Mennucci, G. A. Petersson, H. Nakatsuji, M. Caricato, Xiaosong Li, H. P. Hratchian, Artur F. Izmaylov, Julien Bloino, G. Zheng, J. L. Sonnenberg, M. Hada, M. Ehara, K. Toyota, R. Fukuda, J. Hasegawa, M. Ishida, T. Nakajima, Y. Honda, O. Kitao, H. Nakai, T. Vreven, J. A. Montgomery Jr., J. E. Peralta, François Ogliaro, Michael J. Bearpark, Jochen Heyd, E. N. Brothers, K. N. Kudin, V. N. Staroverov, Rika Kobayashi, J. Normand, Krishnan Raghavachari, Alistair P. Rendell, J. C. Burant, S. S. Iyengar, Jacopo Tomasi, M. Cossi, N. Rega, N. J. Millam, M. Klene, J. E. Knox, J. B. Cross, V. Bakken, C. Adamo, J. Jaramillo, R. Gomperts, R. E. Stratmann, O. Yazyev, A. J. Austin, R. Cammi, C. Pomelli, J. W. Ochterski, R. L. Martin, K. Morokuma, V. G. Zakrzewski, G. A. Voth, P. Salvador, J. J. Dannenberg, S. Dapprich, A. D. Daniels, Ö. Farkas, J. B. Foresman, J. V. Ortiz, J. Cioslowski and D. J. Fox, *Gaussian 09, Revision E.01* , Gaussian, Inc., Wallingford, CT, USA, 2009 .
50. T. A. Keith, *AIMAll, Revision 17.01.25* , TK Gristmill Software, Overland Park KS, USA, 2017 .